NOAA Technical Memorandum ERL WPL-226

ADVANTAGES OF TAPERING FINITE DATA RECORDS FOR SPECTRAL ANALYSIS

L. Kristensen
P. Kirkegaard
C. W. Fairall
J. C. Kaimal
D. H. Lenschow

Wave Propagation Laboratory
Boulder, Colorado
September 1992

noaa NATIONAL OCEANIC AND ATMOSPHERIC ADMINISTRATION / Environmental Research Laboratories

NOAA Technical Memorandum ERL WPL-226

ADVANTAGES OF TAPERING FINITE DATA RECORDS FOR SPECTRAL ANALYSIS

L. Kristensen
P. Kirkegaard
C. W. Fairall
J. C. Kaimal
D. H. Lenschow

Wave Propagation Laboratory
Boulder, Colorado
September 1992

UNITED STATES DEPARTMENT OF COMMERCE

Barbara Hackman Franklin
Secretary

NATIONAL OCEANIC AND ATMOSPHERIC ADMINISTRATION

John A. Knauss
Under Secretary for Oceans and Atmosphere/Administrator

Environmental Research Laboratories

Joseph O. Fletcher
Director

NOTICE

Mention of a commercial company or product does not constitute an endorsement by the NOAA Environmental Research Laboratories. Use of information from this publication concerning proprietary products or the tests of such products for publicity or advertising purposes is not authorized.

For sale by the National Technical Information Service, 5285 Port Royal Road
Springfield, VA 22061

CONTENTS

Page

Abstract 1

1. Introduction 2

2. Theoretical background 4

2.1 Infinite, continuous time series 4

2.2 Finite, discrete sampling 5

2.3 Sample spectra 6

2.4 The continuous limit 10

2.5 Effect on covariances 12

3. Application to power-law spectra 14

4. Examples 23

4.1 Synthetic time series 23

4.2 Aircraft data series 24

5. Conclusions 28

References 32

Appendix A. The integral $T(\alpha; m, n)$ 34

ADVANTAGES OF TAPERING FINITE DATA RECORDS FOR SPECTRAL ANALYSIS

L. Kristensen[1] and P. Kirkegaard
Risø National Laboratory
4000 Roskilde, Denmark

C. W. Fairall and J. C. Kaimal
NOAA/ERL Wave Propagation Laboratory
Boulder, Colorado

D. H. Lenschow
National Center for Atmospheric Research
Boulder, Colorado

ABSTRACT

We discuss in general the relation between the "true" spectrum of stationary time series of infinite duration and that obtained by digital computation from discretely sampled, real time-series of finite duration. In particular, we investigate the effect of an arbitrary time weighting function $h(t)$ applied to the time series (tapering) and illustrate our results by comparing the effect of Hanning tapering with the effect of no tapering in the idealized case of a time series with a power-law spectrum. Our main conclusion is that this spectrum will be seriously distorted without tapering if it falls off with a power greater than 2, and that a Hanning window will restore most of the true spectrum, with the exception of perhaps the first few harmonics, for powers in the interval from +1 to -3, provided the computed spectrum is renormalized by the area under the square of $h(t)$. We also found that in the case when the spectrum falls off with a power greater than 1 this renormalization will be different from the ratio between the variance calculated with and without Hanning tapering. Our predictions are verified using synthetic time series, constructed from discrete 16,384-point power-law spectra and pseudo-randomly created phases, and using aircraft measurements of the longitudinal air velocity component.

---

[1]Visiting with the National Center for Atmospheric Research, Boulder, Colorado.

1 Introduction

The analysis of geophysical data often includes computation of spectra. In many cases, the spectral analysis is performed to determine the characteristic scales of the physical processes of interest, typically indicated by a peak or significant change in slope of the spectrum (e.g., Kaimal 1978). In other cases, the slope of the spectrum is of specific interest. The presence of a particular slope gives information on the dynamics of the system. For example, the inertial subrange of locally isotropic turbulence is characterized by a spectrum with wave number to the $-5/3$ (Lumley and Panofsky 1964), which can be used to estimate the rate of dissipation of turbulent kinetic energy, ϵ. The rate of dissipation is relevant not only to the turbulent dynamics but can also be used for indirect estimates of the turbulent surface fluxes (Fairall and Larsen 1986). Variability due to internal gravity waves in the stratified atmosphere is characterized by a k^{-3} spectrum (Sidi et al. 1988), the viscous-convective subrange by a k^{-1} spectrum (Tennekes and Lumley 1972) and two-dimensional turbulence by a $k^{-5/3}$ spectrum (Charney 1971). The so-called enstrophy cascade in two-dimensional turbulence leads to a k^{-3} dependence (Kraichnan 1967). Anderson (1977) has shown that the spectrum of fluctuations of atmospheric space charge density is characterized by a $k^{-11/3}$ behavior in pristine air but approaches the conventional $k^{-5/3}$ inertial subrange slope for scalars when the charges are attached to aerosol particles. Thus, the relevant dominance of fast ion versus slow ion processes for atmospheric electrical interactions can be determined by a simple measurement of the slope of the spectrum of fluctuations of charge density (Anderson 1982).

"The spectrum" is an abstraction or idealization; it is possible to define it under very restricted conditions that, at best, can only be approximated experimentally. Thus, the theoretical descriptions of turbulence physical processes are made with the tools of the theoretician, who talks of "an ensemble of infinite time series obeying strict ergodicity, stationarity, homogeneity,...", and performs elegant mathematical manipulations with Fourier transforms. The experimentalist deals with a limited time series of discrete points. This sample of data can provide only an estimate of the intrinsic properties of the system, including the "true" spectrum or the "true" spectral slope. The time series is massaged or preprocessed in various ways (mean subtraction, linear trend removal, tapering, etc.) to improve the quality of the estimate of the spectrum in the range of interest. By necessity our samples are finite, but convenience or computational speed requirements often lead to the computation of a spectral estimate as the average of a number of short segments. For example, data from the Boulder Atmospheric Observatory (BAO) are archived at 20-min intervals (Kaimal and Gaynor 1983). Fairall et al. (1990) describe a system for real-time computations of inertial subrange spectra of velocity, temperature, and humidity that ignores frequencies less than 2 Hz.

The effect of a finite sample on the signal variance is well understood (e.g., Pasquill and Smith 1983), but considerable confusion about the spectral implications still exists (e.g.,

Hasse 1985). These problems are often ignored by assuming a "spectral gap" conveniently located at time scales longer than our sample time (e.g., see the discussion in Chapter 4 of Panofsky and Dutton 1984). Kaimal et al. (1989) took a major step forward on this issue when they showed that a spectrum computed from a segment sampled with the rectangular window (i.e., no tapering) would be quite different from the intrinsic spectrum characteristic of the infinite time series if the segment length were not much longer than the integral time scale. Kristensen and Kirkegaard (1989) showed that the pseudo-transfer function representing the finite sample-length effect depends on the rate at which the spectrum rolls off at the high end. It converges to unity as frequency approaches infinity for powers greater than -2, is constant for a -2 spectrum, and diverges for powers less than -2. This distortion of the spectrum computed for finite samples is caused by "leakage" of low frequency energy into the spectral range of interest (Kaimal et al. 1989). Using an 80-min time series of vertical velocity, with a sampling rate of 10 s^{-1}, Kaimal and Kristensen (1990) empirically showed that the leakage effect can be greatly reduced by removing the mean and applying a window to each short segment of the time series, which was consistent with the findings of Fairall et al. (1990). Kaimal and Kristensen (1990) examined six standard windows and found that the Hamming and Hanning (or von Hann) windows (Hamming 1977) yielded the most faithful reproductions of the intrinsic spectrum.

In this paper we focus on the importance of the choice of the specific window used to sample the time series. In contrast to Kaimal et al. (1989), who made a preliminary analysis of a more complicated and specific case, an atmospheric turbulence spectrum with a clearly defined integral time scale, we examine the conceptually simplest spectral model, the infinite continuous spectrum described by a power law. This strict power-law spectrum does not possess an integral time scale. It is also characterized by infinite variance, but this does not cause any theoretical problems. If the power is negative, then our finite sample will contain finite variance. If the power law is positive, then even a finite sample has infinite variance, but we know that any real measurement method must act as a low-pass filter and limit the variance. From a practical point of view, the fact that the physical process we are studying does not possess a fixed power law spectrum over all ranges of frequencies is also not a problem. We are really interested in the question, "If the intrinsic spectrum is characterized by a power law in some frequency range, how do we process the data to obtain an accurate representation of the real power law?"

We use a "top-down" approach to examine this question. We begin by discussing the infinite and continuous time series whose spectrum is described in terms of the infinite and continuous Fourier transform. We then extract from the infinite time series a record of finite length and restrict the sample to discrete points (finite, discrete Fourier series) that represent standard digital measurements. Finally, to simplify the equations and exclude the number of sample points as a parameter, we let the number of sample points go to infinity. This corresponds to the well-known Fourier series approach in which spectral aliasing is absent. We investigate the relative merits of the rectangular window versus the Hanning window. There is no need to study a series of different windows because one well-chosen

tapering window is sufficient to show its advantages over the rectangular window.

2 Theoretical background

To provide the mathematical basis for our study and define our notation, in this section we discuss various basic concepts. First, we state the formal definition of spectra, which require infinite, continuous time series. Second, we discuss finite time series, sampled equidistantly at a finite number of points, and introduce the window concept. Third, we establish the connection between digitally computed spectra and the formally defined spectra. This, in turn, leads in a natural way to the definition of spectral aliasing. Fourth, we study the limit of infinite temporal resolution of finite time series and, finally, the effect of tapering windows on covariances.

2.1 Infinite, continuous time series

As pointed out, to define a spectrum we need an ensemble of stationary, random time series of infinite duration. The ensemble must consist of infinitely many members or realizations. Each realization is a pair of real time series, $x(t)$ and $y(t)$, which may or may not be the same. We assume, without loss of generality, that the ensemble averages of $x(t)$ and $y(t)$ are zero, viz.

$$\langle x(t) \rangle = \langle y(t) \rangle = 0,$$

where angle brackets here and in the following denote ensemble averaging. Because $x(t)$ and $y(t)$ are random time series, they are not in general integrable.

The cross-covariance function is defined as

$$R_{xy}(\tau) = \langle x(t - \tau/2) y(t + \tau/2) \rangle. \tag{1}$$

(The time series are stationary, implying that $R_{xy}(\tau)$ is a function of the time lag τ only and not of "running time" t.) It can be shown (e.g., see Lumley and Panofsky 1964) that the Fourier Integral Theorem applies to the cross-covariance function, so $R_{xy}(\tau)$ can be decomposed as

$$R_{xy}(\tau) = \int_{-\infty}^{\infty} \Phi_{xy}(\omega) e^{i\omega\tau} d\omega, \tag{2}$$

where

$$\Phi_{xy}(\omega) = \frac{1}{2\pi} \int_{-\infty}^{\infty} R_{xy}(\tau) e^{-i\omega\tau} d\tau, \tag{3}$$

by definition, is the cross spectrum of the time series $x(t)$ and $y(t)$.

When $y(t) = x(t)$, then $\Phi_{xy}(\omega) \equiv \Phi(\omega)$ is called the power-spectral density, or just the spectrum, of $x(t)$. It can easily be shown that $\Phi(\omega)$ is real and even. Further, the more formal definition of $\Phi(\omega)$ (Lumley and Panofsky 1964) implies that it is positive definite; i.e., $\Phi(\omega) \geq 0$ for all ω. Note that the autocovariance function $R(\tau) = R_{xx}(\tau) = R_{yy}(\tau)$ is in general not positive definite. The integral time scale $\mathcal{T}$ is defined as

$$\mathcal{T} = \frac{1}{\sigma^2} \int_0^{\infty} R(\tau) d\tau, \tag{4}$$

where

$$\sigma^2 = R(0)$$

is the variance of $x(t)$. It represents the "memory" of the time series; if $\mathcal{T}$ is infinite it means that the autocorrelation function,

$$\rho(\tau) = R(\tau)/\sigma^2,$$

does not go to zero as τ goes to infinity.

2.2 Finite, discrete sampling

To simulate the experimental situation, we now imagine that we select from each member of the infinite ensemble a finite record of duration T and sample this record at N points, spaced equidistantly with the temporal resolution Δt. The spectral resolution, which is defined is terms of the record duration T, is

$$\Delta\omega = \frac{2\pi}{T}. \tag{5}$$

The identities

$$T = N\Delta t = \frac{2\pi}{\Delta\omega} \tag{6}$$

are used many times in the following without being mentioned explicitly.

One single realization is

$$\left\{ \begin{array}{c} x[\ell] \\ y[\ell] \end{array} \right\} = \left\{ \begin{array}{c} x(\ell\Delta t) \\ y(\ell\Delta t) \end{array} \right\}, \quad \ell = -\frac{N}{2}, -\frac{N}{2}+1, \ldots, \frac{N}{2}-1, \tag{7}$$

where we, for convenience, assume that N is even. We subtract the time average

$$\left\{ \begin{array}{c} x_N \\ y_N \end{array} \right\} = \frac{1}{N} \sum_{\ell} \left\{ \begin{array}{c} x[\ell] \\ y[\ell] \end{array} \right\} \tag{8}$$

in each realization before we apply the window. (Here, and in the following, all summations in which the limits are not stated go from $-N/2$ to $N/2-1$.) If this window has no tapering, then this subtraction has no effect on the spectrum, as we shall see.

We assume that $x(t)$ and $y(t)$ are the same type of signal so that it is appropriate to apply the same window

$$h[\ell] = h(\ell\Delta t), \quad \ell = -\frac{N}{2}, -\frac{N}{2}+1, \ldots, \frac{N}{2}-1 \tag{9}$$

to both time series.

The finite, discrete Fourier transform of the two records is

$$\left\{ \begin{array}{c} \hat{x}[k] \\ \hat{y}[k] \end{array} \right\} = \frac{1}{N} \sum_{\ell} h[\ell] \left\{ \begin{array}{c} x[\ell] - x_N \\ y[\ell] - y_N \end{array} \right\} e^{2\pi i \ell k/N}. \tag{10}$$

To obtain the spectral estimates, we multiply $\hat{x}[k]$ by $\hat{y}^*[k]$, indicating complex conjugation with an asterisk. After this we usually smooth, which is band averaging of the raw spectral estimates over a number of consecutive values of the harmonic number k. If the same band width M is applied through the entire range of k from $k = 1$ to $k = N/2$, the last corresponding to the Nyquist frequency, the smoothing procedure is almost equivalent to subdividing the original time series into M sections of the same lengths to approximate an ensemble and then determine an ensemble average of $\hat{x}[k]\hat{y}^*[k]$. If each segment is long compared to the integral scale, i.e., $N\Delta t/M \gg \mathcal{T}$, so that they can be considered approximately statistically independent, this ensemble is considered an approximation to a real ensemble, which, as we have pointed out, is a mathematical abstraction.

2.3 Sample spectra

In the next section we discuss time series with spectra that are power laws in an infinite frequency band $0 < |\omega| < \infty$. Such time series have infinite integral scale (and infinite variance) and are of course themselves mathematical abstractions. For now we are assuming

the existence of an ensemble of this type of time series in order to derive conclusions about the average behavior of spectra and cross spectra of time series subjected to windowing.

We define

$$\Psi_{xy}[k;N] \equiv \langle \hat{x}[k]\hat{y}^*[k] \rangle \tag{11}$$

and substitute (10) to obtain

$$\begin{aligned}\Psi_{xy}[k;N] &= \frac{1}{N}\sum_{\ell'} h[\ell']e^{2\pi i\ell' k/N}\frac{1}{N}\sum_{\ell''} h[\ell'']e^{-2\pi i\ell'' k/N} \\ &\times \left\{ R_{xy}(\{\ell''-\ell'\}\Delta t) + \frac{1}{N}\sum_{m'}\frac{1}{N}\sum_{m''} R_{xy}(\{m''-m'\}\Delta t) \right. \\ &- \left. \frac{1}{N}\sum_{m'} R_{xy}(\{\ell''-m'\}\Delta t) - \frac{1}{N}\sum_{m''} R_{xy}(\{m''-\ell'\}\Delta t) \right\},\end{aligned} \tag{12}$$

where we used (8) and the definition (1) of the cross-covariance function.

At this point we introduce the hybrid Fourier transform

$$\hat{h}_N(\omega) = \frac{1}{N}\sum_{\ell} h[\ell]e^{i\omega\ell\Delta t}, \tag{13}$$

which is a generalization of

$$\hat{h}_N[k] = \frac{1}{N}\sum_{\ell} h[l]e^{2\pi i\ell k/N} \tag{14}$$

with the inverse transform

$$h[\ell] = \sum_{k} \hat{h}_N[k]e^{-2\pi i\ell k/N}, \tag{15}$$

and substitute (2) into (12), followed by interchanging of integration and summation to obtain

$$\Psi_{xy}[k;N] = \int_{-\infty}^{\infty} H_N(k,\omega)\Phi_{xy}(\omega)d\omega, \tag{16}$$

where

$$H_N(k,\omega) = \left| \hat{h}_N(\omega_k-\omega) - \hat{h}_N(\omega_k)\exp\left(i\frac{\omega T}{2N}\right)\frac{\sin\left(\frac{\omega T}{2}\right)}{N\sin\left(\frac{\omega T}{2N}\right)} \right|^2 \tag{17}$$

with

$$\omega_k \equiv k\Delta\omega.$$

Equations (16) and (17) are the fundamental relations connecting the discrete cross-spectrum $\Psi_{xy}[k;N]$ to the idealized, theoretical cross-spectrum $\Phi_{xy}(\omega)$.

Considering the case of no tapering for which

$$h[\ell] = 1,$$

we have

$$\hat{h}_N(\omega) = \exp\left(-i\frac{\omega T}{2N}\right)\frac{\sin\left(\frac{\omega T}{2}\right)}{N\sin\left(\frac{\omega T}{2N}\right)}. \tag{18}$$

For the special values $\omega = \omega_k = k \times 2\pi/T$, we get

$$\hat{h}_N(\omega_k) = \delta_{k,0}, \tag{19}$$

where we introduced the Kronecker delta

$$\delta_{k,m} = \begin{cases} 1 & \text{for } k = m \\ 0 & \text{for } k \neq m \end{cases}. \tag{20}$$

Since we never use the element $k = 0$, for no tapering we get

$$H_N(k,\omega) = \frac{\sin^2\left(\frac{\omega_k-\omega}{2}T\right)}{N^2\sin^2\left(\frac{\omega_k-\omega}{2N}T\right)}. \tag{21}$$

This function describes the well-known spectral aliasing because $H_N(k,\omega)$ for sufficiently large values of N is often conveniently approximated by the so-called Dirac comb

$$H_N(k,\omega) \approx \Delta\omega \sum_{m=-\infty}^{\infty} \delta(\omega_k - \omega + m2\omega_N), \tag{22}$$

where

$$\omega_N = \frac{\pi}{\Delta t}$$

is the Nyquist frequency and

$$\delta(s) = \frac{1}{\pi} \lim_{K \to \infty} \frac{\sin(Ks)}{s} \tag{23}$$

the Dirac delta function.

Substituting (22) into (16) yields

$$\Psi_{xy}[k;N] \approx \Delta\omega \sum_{m=-\infty}^{\infty} \Phi_{xy}(\omega_k + m2\omega_N). \tag{24}$$

In this description of spectral aliasing we assumed that the finite width of the all the main peaks in the entire infinite frequency domain can be neglected. We shall see in section 3 that this assumption does not always give correct results.

If the temporal resolution Δt is so good that the contributions to $\Psi_{xy}[k;N]$ from terms with $m \neq 0$ can be neglected, except perhaps when ω_k is very close to ω_N, then

$$\Psi_{xy}[k;N] \approx \Delta\omega\Phi_{xy}(\omega_k), \quad |\omega_k| < \omega_N, \tag{25}$$

which means that

$$H_N(k,\omega) \approx \Delta\omega\delta(\omega_k - \omega), \quad |\omega_k| < \omega_N \tag{26}$$

for no tapering.

If $h[\ell]$ is different from unity we characterize $h[\ell]$ as a "good" window if

$$H_N(k,\omega) \approx C\Delta\omega\delta(\omega_k - \omega), \quad |\omega_k| < \omega_N, \tag{27}$$

where C is a frequency-independent constant.

When $|\omega_k|$ is more than a few times $\Delta\omega$, the dominant term in (17) is $\hat{h}_N(\omega_k - \omega)$ and the general expression for $H_N(k,\omega)$ can be approximated as

$$H_N(k,\omega) \approx |\hat{h}_N(\omega_k - \omega)|^2. \tag{28}$$

Combining (27) and (28) and integrating over ω, we get

$$C\Delta\omega \approx \int_{-\omega_N}^{\omega_N} |\hat{h}_N(\omega_k - \omega)|^2 d\omega, \tag{29}$$

which, with the aid of (13), can be written as

$$\begin{aligned} C\Delta\omega &\approx \frac{1}{N}\sum_{\ell'} h[\ell']\frac{1}{N}\sum_{\ell''} h[\ell'']e^{i\omega_k(\ell''-\ell')\Delta t}\int_{-\pi/\Delta t}^{\pi/\Delta t} e^{-i\omega(\ell''-\ell')\Delta t}d\omega \\ &= \frac{1}{N}\sum_{\ell'} h[\ell']\frac{1}{N}\sum_{\ell''} h[\ell'']\frac{2\pi}{\Delta t}\delta_{\ell',\ell''} = \frac{2\pi}{T}\frac{1}{N}\sum_{\ell} h^2[\ell], \end{aligned} \tag{30}$$

so that

$$C = \frac{1}{N}\sum_{\ell} h^2[\ell]. \tag{31}$$

Keeping T fixed and letting $N \to \infty$, we have in general for any function $f(t)$ in the time domain

$$\lim_{N\to\infty}\left\{\frac{1}{N}\sum_{\ell} f[l]\right\} = \frac{1}{T}\int_{-T/2}^{T/2} f(t)dt, \tag{32}$$

so that (31) in the limit of infinite temporal resolution becomes

$$C = \frac{1}{T}\int_{-T/2}^{T/2} h^2(t)dt. \tag{33}$$

In other words, the scaling of a spectrum, calculated with a given window $h(t)$, is the area under the square of the window.

To summarize this last result, the cross spectrum $\Psi_{xy}[k;N]$ is roughly proportional to the idealized, theoretical cross spectrum $\Phi_{xy}(\omega_k)$, provided the frequency $\omega_k = k \times 2\pi/T$ is small compared to the Nyquist frequency. However, the relation

$$\Psi_{xy}[k;N] \approx \Phi_{xy}(\omega_k), \tag{34}$$

where C is given by (33), is derived by means of a heuristic analysis and is not always accurate enough for spectral analysis, even with infinite good temporal resolution. As we have seen, there is a general integral relation, that is (16), between $\Phi_{xy}(\omega)$ and $\Psi_{xy}[k;N]$, so that the last is a weighted integral of the first with the weighting function $H_N(k,\omega)$. In the next subsection we derive $H_N(k,\omega)$ in the case of a window with no tapering and a window with Hanning tapering.

2.4 The continuous limit

We imagine that we keep the record duration T constant and let N go to infinity in which case we can neglect spectral aliasing, but we take the finite width of $H_N(k,\omega)$ into account. In this limit we have infinite temporal resolution and (21) becomes

$$H^{\mathrm{nt}}(k,\omega) = \lim_{N\to\infty}\{H_N(k,\omega)\} = \mathrm{sinc}^2\left(k\pi - \frac{\omega T}{2}\right) \equiv \frac{\sin^2\left(k\pi - \frac{\omega T}{2}\right)}{\left(k\pi - \frac{\omega T}{2}\right)^2}, \tag{35}$$

where the superscript nt denotes no tapering.

This result could have been obtained immediately from the main equation in Kaimal et al. (1989), which is derived for continuous spectra of finite time series. If in their eq. (13) we let the frequency f be a multiple of T^{-1}, as we assume here, the result is the same as that given by (16) with (35).

In the case of Hanning tapering we have (Harris 1978)

$$h[\ell] = \cos^2\left(\pi\frac{\ell\Delta t}{T}\right) = \frac{1}{4}\left\{2 + \exp\left(2\pi i\frac{\ell\Delta t}{T}\right) + \exp\left(-2\pi i\frac{\ell\Delta t}{T}\right)\right\} \tag{36}$$

and

$$\begin{aligned}\hat{h}_N(\omega) \;=\; & \frac{1}{4}\left\{2\exp\left(-i\frac{\omega T}{2N}\right)\frac{\sin\left(\frac{\omega T}{2}\right)}{N\sin\left(\frac{\omega T}{2N}\right)}\right. \\ & + \exp\left(-i\frac{\omega T + 2\pi}{2N}\right)\frac{\sin\left(\frac{\omega T+2\pi}{2}\right)}{N\sin\left(\frac{\omega T+2\pi}{2N}\right)} \\ & \left. + \exp\left(-i\frac{\omega T - 2\pi}{2N}\right)\frac{\sin\left(\frac{\omega T-2\pi}{2}\right)}{N\sin\left(\frac{\omega T-2\pi}{2N}\right)}\right\}\end{aligned} \tag{37}$$

so that

$$\begin{aligned}H_N(k,\omega) \;=\; & \frac{1}{16}\left|2\exp\left(-i\frac{(\omega_k-\omega)T}{2N}\right)\frac{\sin\left(\frac{(\omega_k-\omega)T}{2}\right)}{N\sin\left(\frac{(\omega_k-\omega)T}{2N}\right)}\right. \\ & + \exp\left(-i\frac{(\omega_k-\omega)T + 2\pi}{2N}\right)\frac{\sin\left(\frac{(\omega_k-\omega)T+2\pi}{2}\right)}{N\sin\left(\frac{(\omega_k-\omega)T+2\pi}{2N}\right)} \\ & + \exp\left(-i\frac{(\omega_k-\omega)T - 2\pi}{2N}\right)\frac{\sin\left(\frac{(\omega_k-\omega)T-2\pi}{2}\right)}{N\sin\left(\frac{(\omega_k-\omega)T-2\pi}{2N}\right)} \\ & \left. - \delta_{k,1}\exp\left(i\frac{\omega T}{2N}\right)\frac{\sin\left(\frac{\omega T}{2}\right)}{N\sin\left(\frac{\omega T}{2N}\right)}\right|^2.\end{aligned} \tag{38}$$

Again, we want to exclude the effect of spectral aliasing and let N go to infinity, keeping T fixed. This rather complicated equation reduces to

$$\begin{aligned}H^{\mathrm{hn}}(k,\omega) \;=\; & \frac{1}{16}\left\{2\mathrm{sinc}\left(k\pi - \frac{\omega T}{2}\right) + \mathrm{sinc}\left((k+1)\pi - \frac{\omega T}{2}\right)\right. \\ & \left. + \mathrm{sinc}\left((k-1)\pi - \frac{\omega T}{2}\right) - \delta_{k,1}\mathrm{sinc}\left(\frac{\omega T}{2}\right)\right\}^2,\end{aligned} \tag{39}$$

where the superscript hn denotes Hanning.

2.5 Effect on covariances

The finite duration of the time series we are discussing reduces the covariance compared to the covariance of the infinite time series simply because variations with periods longer than T have been reduced significantly. If we apply a tapering window we modify the covariance even more. Consequently, to compare the effects of different windows on the cross-spectra and normalize them to the same covariance, we must calculate the area μ_{xy} under the co-spectra using the windows under investigation.

The easiest way to determine μ_{xy} seems to be to sum $\Psi_{xy}[k;N]$, given by (12), over k from $-N/2$ to $N/2-1$, excluding $k=0$, and then let N go to infinity, keeping T constant. Even this procedure is quite cumbersome, so we just point out the steps to be taken.

Since (12) is formally periodic in k with the period N, it is a little easier to carry out the summation from 0 to $N-1$. We have

$$\mu_{xy} = \sum_{k=0}^{N-1} \Psi_{xy}[k;N] - \Psi_{xy}[0;N]. \tag{40}$$

Using (16), this quantity can be written

$$\mu_{xy} = \int_{-\infty}^{\infty} F(\omega)\Phi_{xy}(\omega)d\omega, \tag{41}$$

where

$$F(\omega) = \sum_{k=0}^{N-1} H_N(k,\omega) - H_N(0,\omega). \tag{42}$$

Equation (41) is the fundamental relation linking the covariance μ_{xy} to the idealized, theoretical cross spectrum $\Phi_{xy}(\omega)$. We evaluate $F(\omega)$ for no tapering and the Hanning window cases.

Equation (12) implies

$$\begin{aligned}\sum_{k=0}^{N-1} H_N(k,\omega) &= \frac{1}{N}\sum_{\ell} h^2[\ell]\left\{1 + \frac{\sin^2\left(\frac{\omega T}{2}\right)}{N^2\sin^2\left(\frac{\omega T}{2N}\right)}\right\} \\ &\quad - 2\frac{\sin\left(\frac{\omega T}{2}\right)}{N\sin\left(\frac{\omega T}{2N}\right)}\frac{1}{N}\sum_{\ell} h^2[\ell]\cos\left(\omega\ell\Delta t + \frac{\omega T}{2N}\right),\end{aligned} \tag{43}$$

and from (17) we get

$$H_N(0,\omega) = \left| \hat{h}_N(\omega) - \hat{h}_N(0) \exp\left(-i\frac{\omega T}{2N}\right) \frac{\sin\left(\frac{\omega T}{2}\right)}{N \sin\left(\frac{\omega T}{2N}\right)} \right|^2 . \tag{44}$$

In the limit $N \to \infty$ (43) and (44) become

$$\begin{aligned} \lim_{N\to\infty} \left\{ \sum_{k=0}^{N-1} H_N(k,\omega) \right\} &= \left\{ 1 + \mathrm{sinc}^2\left(\frac{\omega T}{2}\right) \right\} \frac{1}{T} \int_{-T/2}^{T/2} h^2(t)dt \\ &\quad - 2\mathrm{sinc}\left(\frac{\omega T}{2}\right) \frac{1}{T} \int_{-T/2}^{T/2} h^2(t)\cos(\omega t)dt \end{aligned} \tag{45}$$

and

$$\lim_{N\to\infty} \{H_N(0,\omega)\} = \left| \hat{h}(\omega) - \hat{h}(0)\mathrm{sinc}\left(\frac{\omega T}{2}\right) \right|^2 , \tag{46}$$

where

$$\hat{h}(\omega) = \frac{1}{T} \int_{-T/2}^{T/2} h(t) e^{i\omega t} dt. \tag{47}$$

In the case of no tapering we have $h^{\mathrm{nt}}(t) = 1$ and

$$\hat{h}^{\mathrm{nt}}(\omega) = \mathrm{sinc}\left(\frac{\omega T}{2}\right). \tag{48}$$

Substitution in (45) and (46) yields immediately

$$F^{\mathrm{nt}}(\omega) = 1 - \mathrm{sinc}^2\left(\frac{\omega T}{2}\right), \tag{49}$$

as expected.

The Hanning case is a little more complicated. Here

$$h^{\mathrm{hn}}(t) = \cos^2\left(\pi \frac{t}{T}\right), \tag{50}$$

and its transform becomes

$$\hat{h}^{\mathrm{hn}}(\omega) = \frac{1}{4} \left\{ 2\mathrm{sinc}\left(\frac{\omega T}{2}\right) + \mathrm{sinc}\left(\frac{\omega T}{2} + \pi\right) + \mathrm{sinc}\left(\frac{\omega T}{2} - \pi\right) \right\}. \tag{51}$$

Evaluating (42), we substitute (50) in (45) and (51) in (46). The result is

$$\begin{aligned} F^{\mathrm{hn}}(\omega) &= \frac{3}{8}\left\{1-\mathrm{sinc}^2\left(\frac{\omega T}{2}\right)\right\} \\ &\quad -\frac{1}{2}\mathrm{sinc}\left(\frac{\omega T}{2}\right)\left\{\mathrm{sinc}\left(\frac{\omega T}{2}+\pi\right)+\mathrm{sinc}\left(\frac{\omega T}{2}-\pi\right)\right\} \\ &\quad -\frac{1}{8}\mathrm{sinc}\left(\frac{\omega T}{2}\right)\left\{\mathrm{sinc}\left(\frac{\omega T}{2}+2\pi\right)+\mathrm{sinc}\left(\frac{\omega T}{2}-2\pi\right)\right\} \\ &\quad -\frac{1}{16}\left\{\mathrm{sinc}\left(\frac{\omega T}{2}+\pi\right)+\mathrm{sinc}\left(\frac{\omega T}{2}-\pi\right)\right\}^2. \end{aligned} \tag{52}$$

3 Application to power-law spectra

We now study in more detail the effect of the two windows, both of duration T, on power-law spectra. The first window has no tapering, and the second has a Hanning tapering. As in the preceding section, the "mother" time series $x(t) = y(t)$ is assumed to start at $T = -\infty$ and end at $T = \infty$ and to have the spectrum

$$\Phi(\omega) = A|\omega|^{-\alpha}, \qquad 0 < |\omega| < \infty, \tag{53}$$

where A is a constant.

Time series with this property are of course highly unrealistic, but to reduce this investigation to a one-parameter study (parameter α), we do not wish to include, e.g., the integral time scale $\mathcal{T}$, just as we take our equations to the limit of infinite temporal resolution ($N \to \infty$). In this way we believe that we can reveal important properties of time windows with and without tapering, because the decision to use tapering on real data often must be taken when T is not much larger than $\mathcal{T}$.

We define

$$\Psi(\omega_k; T) \equiv \lim_{N\to\infty} \frac{\Psi[k;N]}{\Delta\omega} \tag{54}$$

and, inserting in (16), we get

$$\Psi(\omega_k; T) = \frac{T}{2\pi}\int_{-\infty}^{\infty} H(k,\omega)\Phi(\omega)d\omega, \tag{55}$$

where $H(k,\omega)$ is given by (35) or (39).

We can now derive a pseudo-transfer function

$$K(k;\alpha) = \frac{\Psi(\omega_k;T)}{\Phi(\omega_k)}, \qquad k = 1,2,\ldots\infty, \tag{56}$$

which describes, with α as a parameter, how the "true" spectrum is modified at all harmonics by the window. Ideally, we would like $K(k;\alpha)$ to be a constant, independent of k. Since $K(k;\alpha)$ is dependent on the spectrum, it is not really a transfer function. We note that with a power-law spectrum as given by (53), $K(k;\alpha)$ is independent of the duration T of the window.

We first derive the pseudo-transfer function for no tapering.

Substituting (35) and (53) in (55), we obtain, by entering that result together with (53) in (56),

$$K^{\mathrm{nt}}(k;\alpha) = k^{\alpha}\pi^{\alpha-1}\int_0^{\infty}\left\{\mathrm{sinc}^2(u+k\pi)+\mathrm{sinc}^2(u-k\pi)\right\}u^{-\alpha}du. \tag{57}$$

When we evaluate the pseudo-transfer function for the Hanning window we need a function of the general form

$$\begin{aligned} T(\alpha;m,n) \;=\; & \pi^{\alpha-1}\int_0^{\infty} u^{-\alpha}\{\mathrm{sinc}(u+m\pi)\mathrm{sinc}(u+n\pi) \\ & \qquad + \mathrm{sinc}(u-m\pi)\mathrm{sinc}(u-n\pi)\}\,du, \end{aligned} \tag{58}$$

which, except when $m = n = 0$, exists in the open interval $-1 < \alpha < 3$. It is shown in the appendix that (58) can be evaluated analytically.

The definition (58) implies

$$T(\alpha;m,n) = T(\alpha;n,m) = T(\alpha;-m,-n). \tag{59}$$

With the tool (58), $K^{\mathrm{nt}}(k;\alpha)$ can be written

$$K^{\mathrm{nt}}(k;\alpha) = k^{\alpha}T(\alpha;k,k). \tag{60}$$

Equations (A33) and (A34) in the appendix show that $K^{\mathrm{nt}}(k;0) = 1$ and $K^{\mathrm{nt}}(k;2) = 2$, irrespective of k. Further,

$$\lim_{k\to\infty}\{K^{\mathrm{nt}}(k;\alpha)\} = \begin{cases} 1 & \alpha < 2 \\ \infty & \alpha > 2. \end{cases} \tag{61}$$

In fact, as (A32) - (A39) show, (60) can for $k \to \infty$ be approximated by the asymptotic expression

$$K^{\mathrm{nt}}(k;\alpha) = \begin{cases} 1 - \dfrac{1}{\cos(\pi\alpha/2)\Gamma(\alpha)} \times \dfrac{1}{(2k\pi)^{2-\alpha}} + \dfrac{\alpha\tan(\pi\alpha/2)}{2k\pi} & \alpha \neq 1 \\ 1 + \dfrac{\ln(2k\pi) + \gamma - 1}{k\pi^2} & \alpha = 1 \end{cases}, \tag{62}$$

where

$$\gamma = 0.5772156649\ldots$$

is Euler's constant.

Figures 1 and 2 show $K^{\mathrm{nt}}(k;\alpha)$ for positive and negative values of α, respectively. We see that $K^{\mathrm{nt}}(k;\alpha)$ approaches unity when $\alpha < 1$. This means that the spectrum $\Phi(\omega_k)$ is well represented by $\Psi^{\mathrm{nt}}(\omega_k)$, at least if the first 10 values of k are excluded. In the interval $1 < \alpha < 2$, $K^{\mathrm{nt}}(k;\alpha)$ goes to unity as k goes to infinity, but unacceptably slowly. When $\alpha > 2$, $K^{\mathrm{nt}}(k;\alpha)$ diverges in the limit $k \to \infty$. Clearly, it is worthwhile investigating whether a Hanning tapering can improve the quality of spectral computation.

Going through the same procedure with a Hanning window in the same situation, we determine $K^{\mathrm{hn}}(k;\alpha)$ using (39). The result is

$$K^{\mathrm{hn}}(k;\alpha) = \frac{k^\alpha}{16} \begin{cases} 4T(\alpha;1,1) + T(\alpha;2,2) + 4T(\alpha;1,2) & k = 1 \\ 4T(\alpha;k,k) + 2T(\alpha;k-1,k+1) & \\ \quad + T(\alpha;k+1,k+1) + T(\alpha;k-1,k-1) & k > 1 \\ \quad + 4T(\alpha;k,k+1) + 4T(\alpha,k,k-1) & \end{cases}. \tag{63}$$

Again, as (A32) through (A39) in the appendix show, this pseudo-transfer function can be written approximately as

$$K^{\mathrm{hn}}(k;\alpha) \approx \frac{3}{8}\left\{1 + \frac{\alpha(\alpha+1)}{6k^2}\right\} \tag{64}$$

for large values of k.

Equation (64) illustrates quite clearly that for all values of α the pseudo-transfer function approaches 3/8 very quickly when k goes to infinity. The reason that it does not approach 1 is that the Hanning window on average suppresses the oscillations of the signal in the time window. Hanning causes a variance loss apart from the loss caused by the finite duration of the time window. We therefore determine how much variance is lost compared to a no-tapering window by substituting first (49) then (52) in (41) (with $y = x$) together with (53).

For no tapering the variance becomes

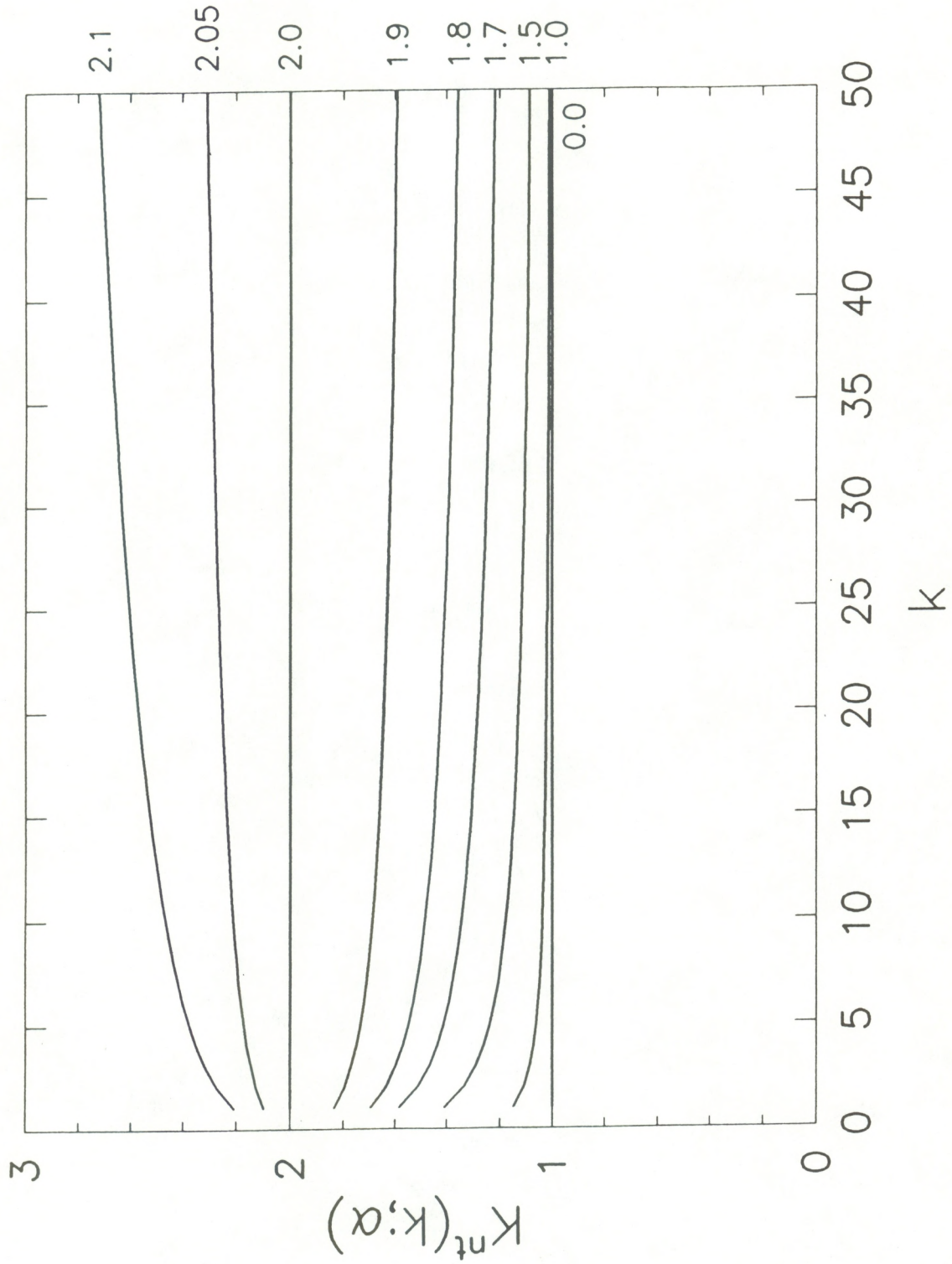

Fig. 1. The pseudo-transfer function $K^{\mathrm{nt}}(k;\alpha)$ for $\alpha \geq 0$ and the harmonics in the interval $1 < k \leq 50$.

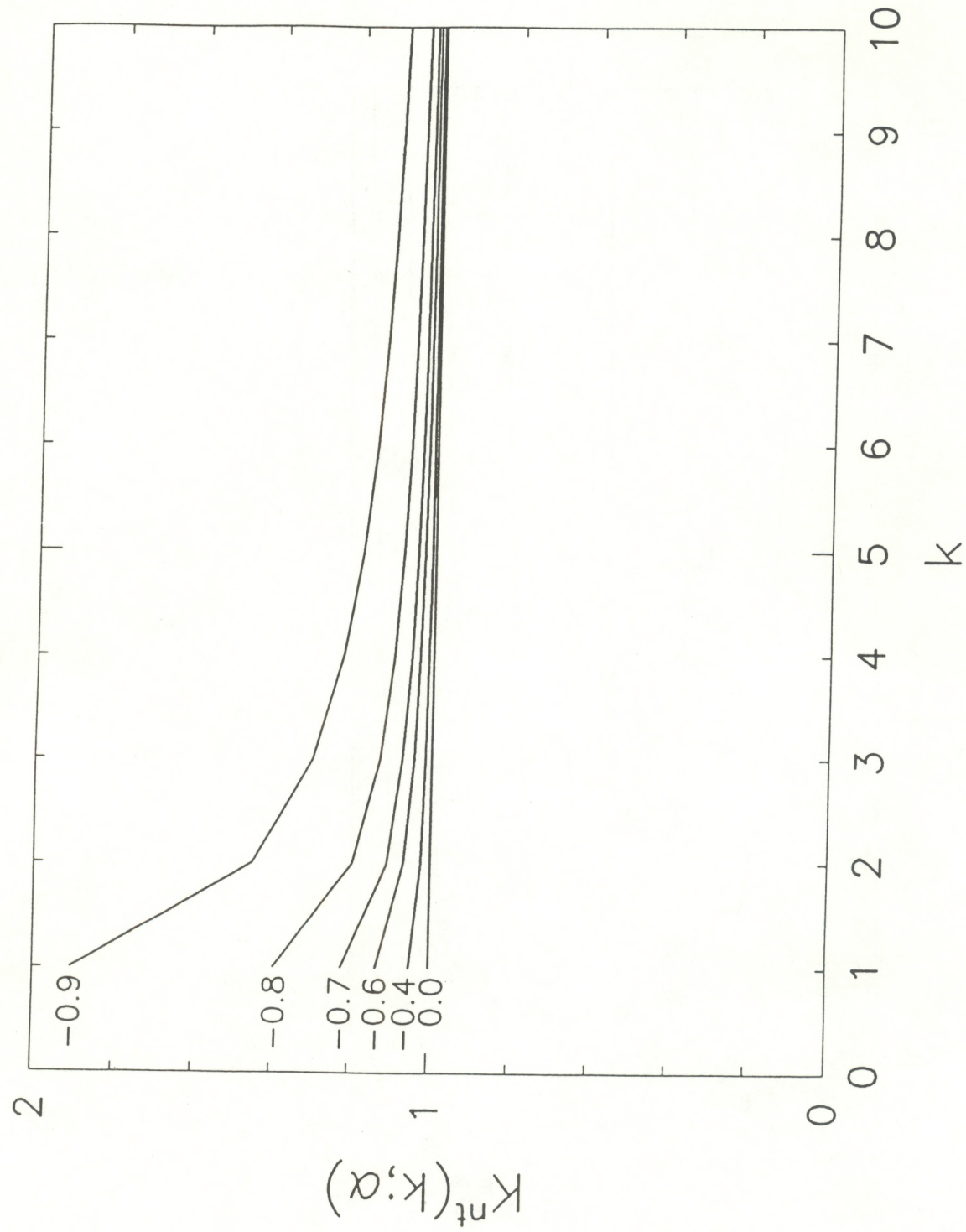

Fig. 2. The pseudo-transfer function $K^{\mathrm{nt}}(k;\alpha)$ for $\alpha \leq 0$ and the harmonics in the interval $1 < k \leq 10$.

$$\sigma^2_{\rm nt}(\alpha) = \int_{-\infty}^{\infty} \left\{1 - \mathrm{sinc}^2\left(\frac{\omega T}{2}\right)\right\} A|\omega|^{-\alpha} d\omega \equiv A\left(\frac{2\pi}{T}\right)^{1-\alpha} \tilde{T}(\alpha), \tag{65}$$

where

$$\tilde{T}(\alpha) = 2\pi^{\alpha-1} \int_0^{\infty} u^{-\alpha}\{1 - \mathrm{sinc}^2(u)\} du = -\frac{(2\pi)^{\alpha}}{\Gamma(2+\alpha)\cos(\pi\alpha/2)}. \tag{66}$$

In a similar way we get

$$\begin{aligned} \sigma^2_{\rm hn}(\alpha) \;=\; & \frac{A}{8}\left(\frac{2\pi}{T}\right)^{1-\alpha} \{3\tilde{T}(\alpha) - 8T(\alpha;0,1) \\ & - 2T(\alpha;0,2) - T(\alpha;1,1) - T(\alpha;1,-1)\}. \end{aligned} \tag{67}$$

The pseudo-transfer function $K^{\rm hn}(k;\alpha)$ must be multiplied by the ratio

$$Q(\alpha) = \frac{\sigma^2_{\rm nt}}{\sigma^2_{\rm hn}} \tag{68}$$

for Hanning not to cause a loss of variance in excess of that caused by the finite record length. In fact, it is a common procedure to perform this correction with experimental time series, where a Hanning procedure preceding the spectral computation is followed by a normalization of the spectral estimate to the variance pertaining to a no-tapering window.

Substituting (65) and (67), we get

$$Q(\alpha) = \left\{\frac{3}{8} - \frac{T(\alpha;0,1)}{\tilde{T}(\alpha)} - \frac{1}{4}\frac{T(\alpha;0,2)}{\tilde{T}(\alpha)} - \frac{1}{8}\frac{T(\alpha;1,1)}{\tilde{T}(\alpha)} - \frac{1}{8}\frac{T(\alpha;1,-1)}{\tilde{T}(\alpha)}\right\}^{-1}. \tag{69}$$

As it is easily seen in (66), $\tilde{T}(\alpha)$ is divergent (infinitely large) when $-1 < \alpha \leq 1$. Because all the T functions are well behaved in the interval $-1 < \alpha < 3$, we conclude that $Q(\alpha)$ is equal to $8/3$ in the interval $-1 < \alpha \leq 1$. The normalization function $Q(\alpha)$ is shown in Fig. 3. We see that $Q(\alpha)$ increases in the interval $1 < \alpha < 3$. This is somewhat disconcerting because (64) shows that the pseudo-transfer function approaches $3/8$ for *all* values of α in the interval $-1 < \alpha < 3$. Since we want as little spectral offset as possible, it seems reasonable always to normalize with $3/8$ for Hanning tapering, at the sacrifice of a loss of variance. This is consistent with (33) because

$$C_{\rm hn} = \frac{1}{T}\int_{-T/2}^{T/2} \cos^4\left(\pi\frac{t}{T}\right) dt = \frac{3}{8}. \tag{70}$$

Figures 4 and 5 show the pseudo-transfer function $K^{\rm hn}(k;\alpha)/C_{\rm hn}$ for positive and negative values of α, respectively.

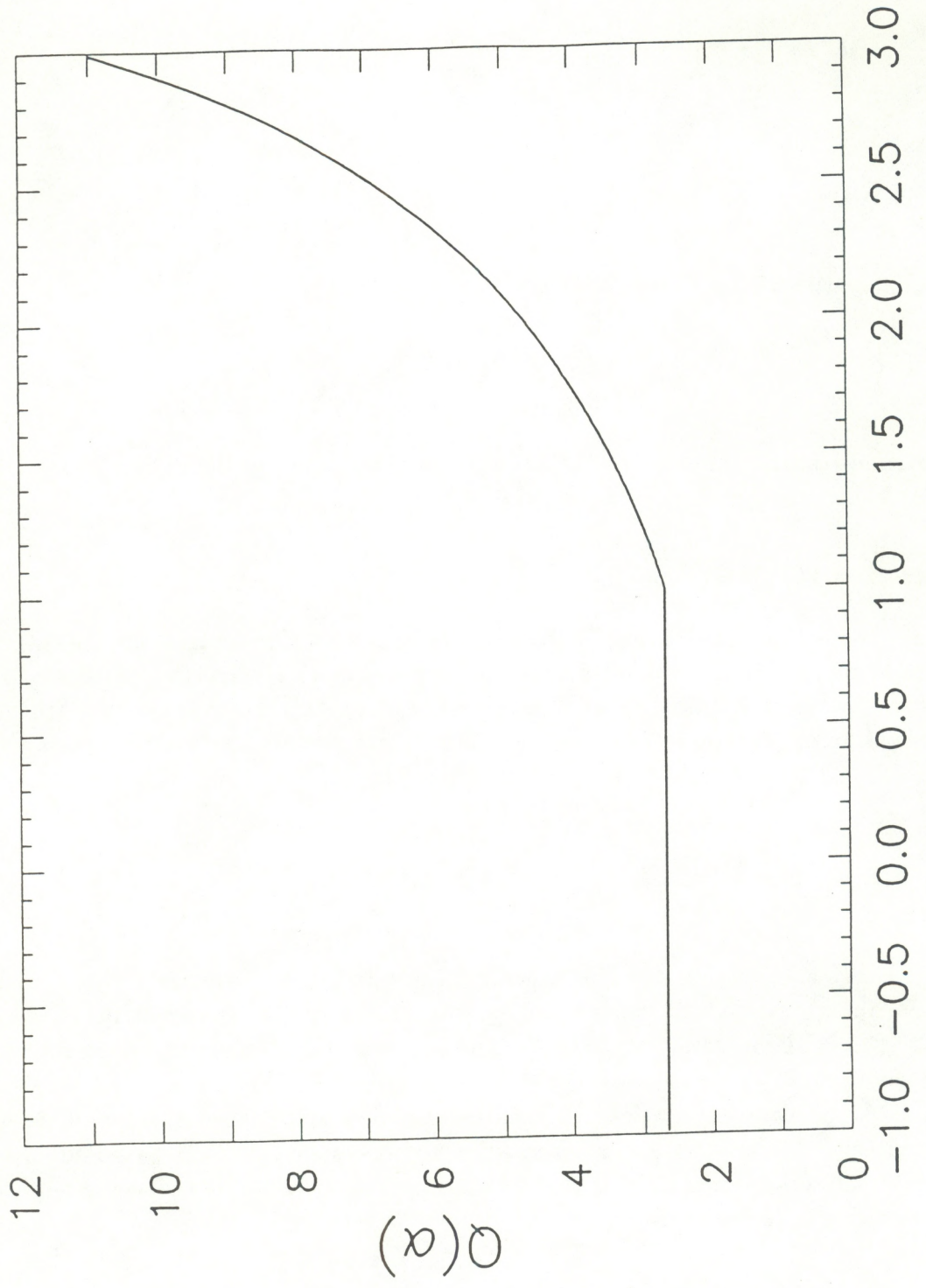

Fig. 3. The ratio $Q(\alpha)$, as function of α between the variance of a time series subjected to a no-tapering window and that of the same time series subjected to a Hanning tapering window.

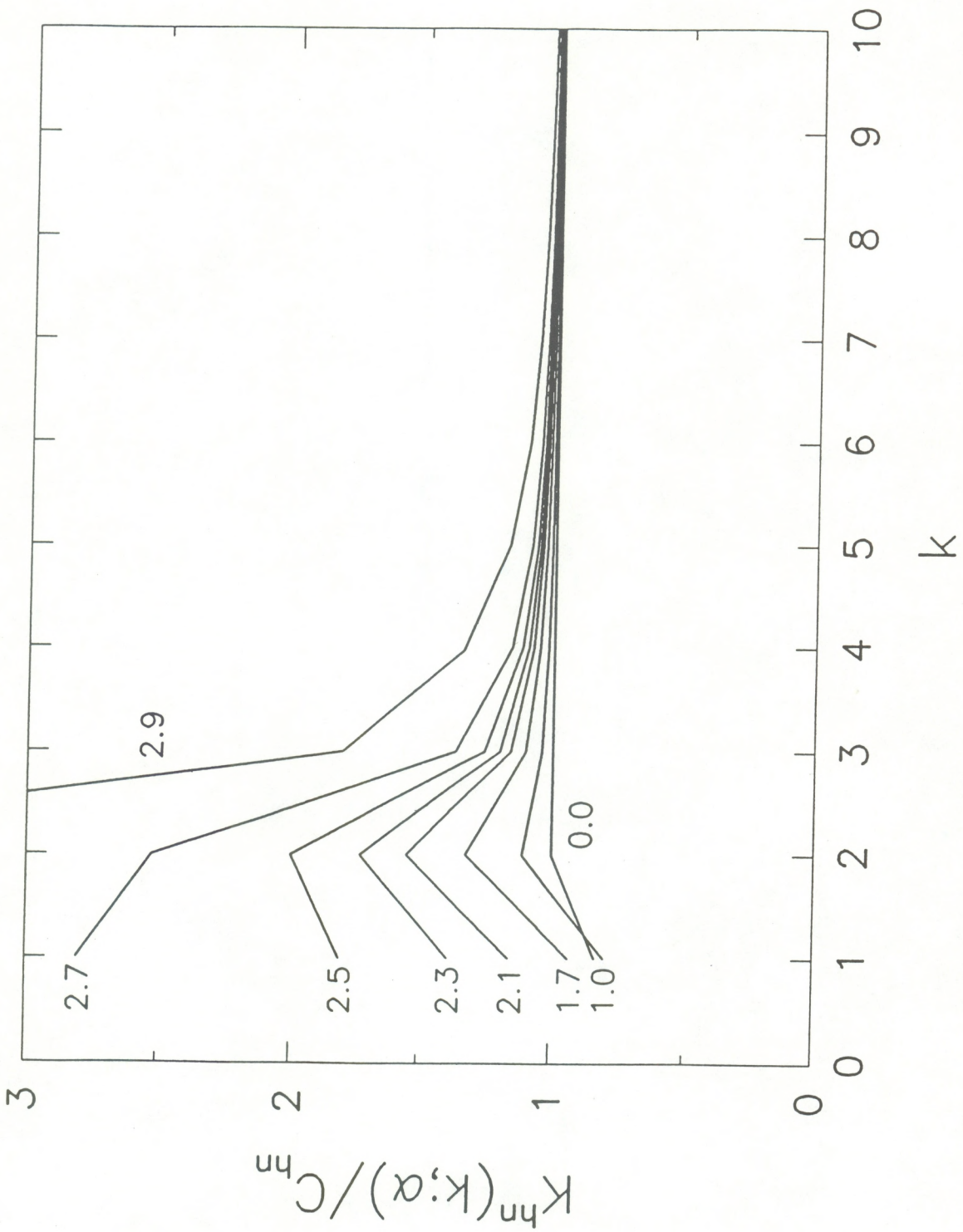

Fig. 4. The pseudo-transfer function $K^{\text{hn}}(k;\alpha)/C_{\text{hn}}$ for $\alpha \geq 0$ and the harmonics in the interval $1 < k \leq 10$.

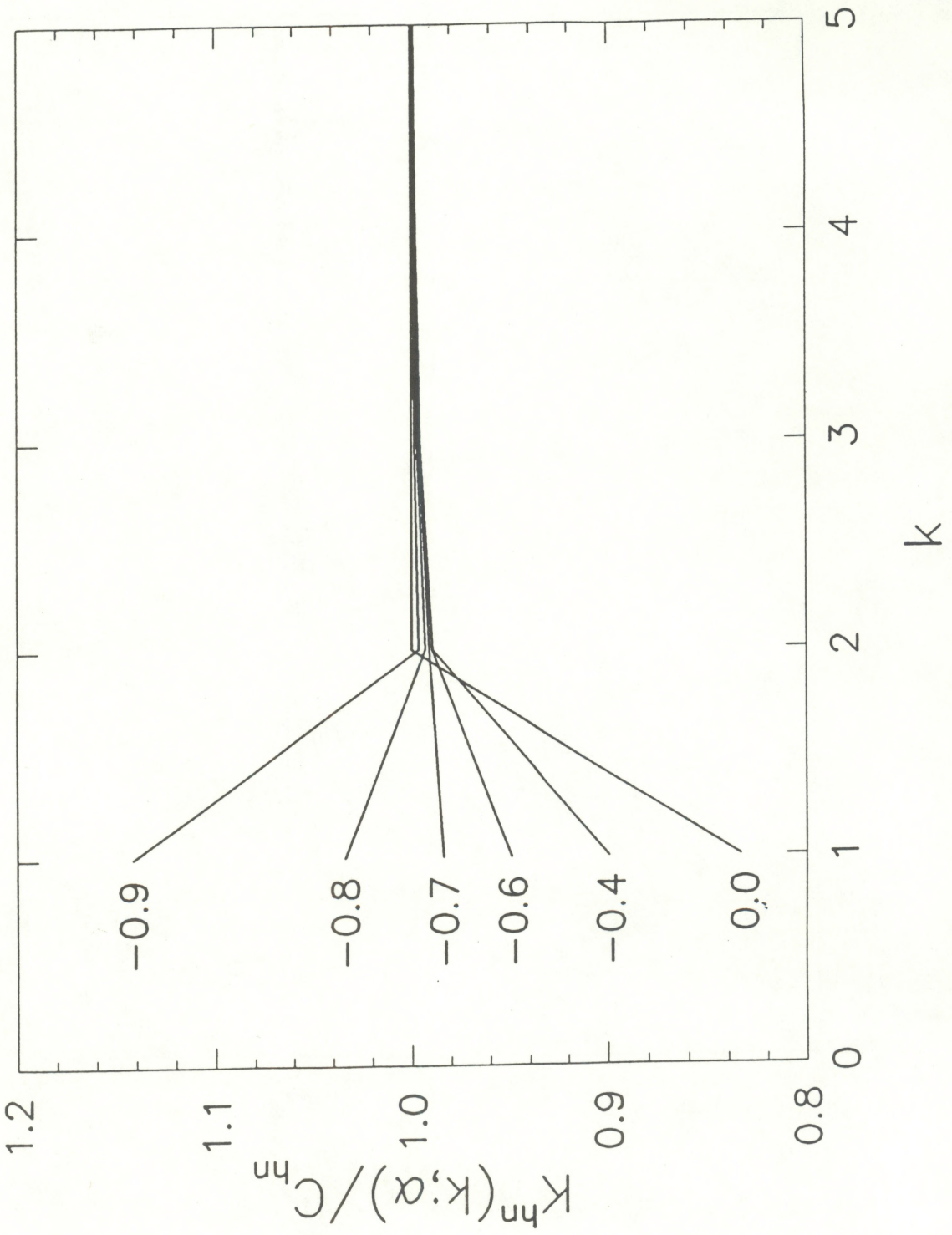

Fig. 5. The pseudo-transfer function $K^{\mathrm{hn}}(k;\alpha)/C_{\mathrm{hn}}$ for $\alpha \leq 0$ and the harmonics in the interval $1 < k < 5$.

4 Examples

In section 2 we developed expressions relating the finite, discrete sampled spectrum to the intrinsic spectrum of an infinite, continuous field and we obtained simplified expressions in the limit of infinite resolution ($N \rightarrow \infty$). These expressions were then applied to the specific case of a power-law spectrum for a rectangular window (no tapering) and a Hanning tapering window (section 3). In this section we compute spectra from finite, discrete time series and compare the results with the theory. We do this comparison for several sets of synthetic time series computed from reverse transforms of pure power-law variance spectra, and for a time series of longitudinal air velocity fluctuations obtained from an aircraft.

4.1 Synthetic time series

We can produce a simulated time series that is automatically characterized by a given power-law variance spectrum by simple Fourier reconstruction:

$$x[\ell] = \sum_k \hat{x}[k] \exp\left(-2\pi i\{\ell k/N + \delta[k]\}\right), \tag{71}$$

where $\hat{x}[k]$ is obtained from the assumed power-law spectral form as

$$\hat{x}[k] = \sqrt{A\Delta\omega|\omega_k|^{-\alpha}}. \tag{72}$$

The quantity $\delta[k]$ is a number between 0 and +1 chosen randomly to give a random phase to each frequency component. Clearly, substitution of (72) into (11) will yield

$$\Phi(\omega_k) = A|\omega_k|^{-\alpha}. \tag{73}$$

Because we are dealing with a finite, discrete system, we cannot synthesize an infinite, continuous time series. Instead, we used (71) and (72) to produce a very long (16,384 points) master realization and we simulated the sampling process discussed earlier by breaking the master realization into N_{ave} individual, short segments of length N ($N \times N_{\text{ave}} = 16,384$). The mean is computed and removed from each short segment, and an estimate of the spectral density from the Nyquist frequency down to the short-segment fundamental frequency (which is N_{ave} times the master fundamental frequency) is computed (with and without applying the tapering window to the short segment). The master time series produces N_{ave} estimates of the spectrum, which are averaged. Twenty separate realizations of the master time series are produced, yielding a final estimate of the intrinsic spectrum computed from 20 N_{ave} samples. Results for $N_{\text{ave}} = 32$ (individual segment lengths of 512 points) are shown

in Figs. 6a-6c and can be compared to the theoretical results in Figs. 1 and 4. The Hanning window results were renormalized by the factor 3/8 as discussed previously. For $\alpha = 1.5$, Fig. 6a clearly shows the extensive distortion of the spectrum by the rectangular window. For $\alpha = 2.0$, Fig. 6b gives the theoretical rectangular window overestimate of $\Phi(\omega_k)$ by a frequency independent factor of 2.0 and $\alpha = 2.1$. Figure 6c shows the rapid divergence of the rectangular window spectral estimates. The Hanning window causes some small distortion at the first few harmonics but thereafter faithfully reproduces the spectrum. The ratios of the rectangular to window-area-corrected Hanning variances are 1.265, 1.622, and 1.735 for α=1.5, 2.0, and 2.1; these values are in close agreement with the theoretical values for $Q(\alpha)$ given in Fig. 3.

4.2 Aircraft data series

Longitudinal air velocity measurements from the NCAR Electra were used to provide an example of a time series of real data. Lenschow (1986) describes the techniques for obtaining the air velocity components from an inertial navigation system and differential pressure measurements on a radome. The time series (sampled at 20 s^{-1}, with the airplane flying at 101 m s^{-1}) were obtained over the sand-hill country of western Nebraska at a height of $\sim$ 30 m above the hill-tops with clear conditions during mid-afternoon on 12 May 1988. Four realizations, each of 16,384 points, were selected. Each realization was linearly detrended and the variance computed before being processed further. A sample 512 point segment of one of these time series is shown in Fig. 7. The variances of the individual realizations differed by $< 20\%$, so we treated the four realizations as belonging to the same ensemble (i.e., we did not normalize the realizations by their standard deviations). The integral time scale, obtained from the average of the four velocity spectra by use of the spectral model developed by Kristensen et al. (1989), was $\mathcal{T} \simeq 49$ s. This differed little from the average of the integral scales for each of the individual realizations.

Each of the four master realizations was subjected to a 16,384-point FFT, the spectral density was computed, the four realizations were averaged, and the resultant average spectrum was subjected to a standard smoothing algorithm. The smoothing was a simple linear average of the spectral densities in a frequency band of a width that increases exponentially with increasing frequency (see Fig. 8). A linear regression was fit to $\log(\omega \times \Phi(\omega))$ versus $\log(\omega)$ in the frequency range between about 0.6 Hz and 60 Hz (dashed line in Fig. 8). The slope of this regression is $1 - \alpha$, the intercept is $\log(A)$. This particular data set yielded $\alpha = 1.479$. This is quite a bit less than the expected value of 5/3 for the inertial subrange of locally isotropic turbulence, but sufficiently large to illustrate spectral distortion by the rectangular window. The four data realizations were processed as described above for the synthetic data. Each master realization was broken into 255 segments of 128 points (i.e., a 50% overlap of adjacent segments). We needed to use more segments to reduce the statistical scatter of the of the overall average spectral estimates. The pseudo-transfer functions

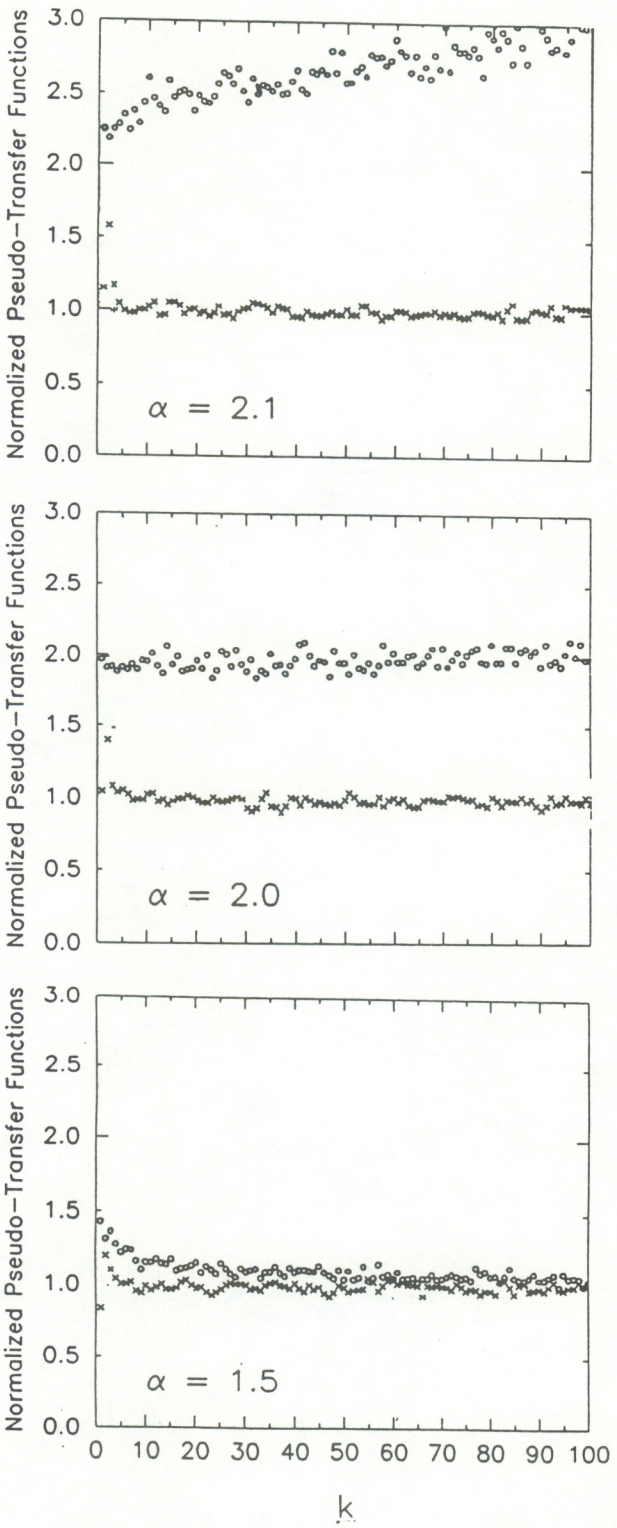

Fig. 6. Normalized pseudo-transfer function versus harmonic index for a synthetic time series. The open circles are the rectangular window and the crosses the Hanning window for (a) α=1.5, (b) α=2.0, and (c) α=2.1.

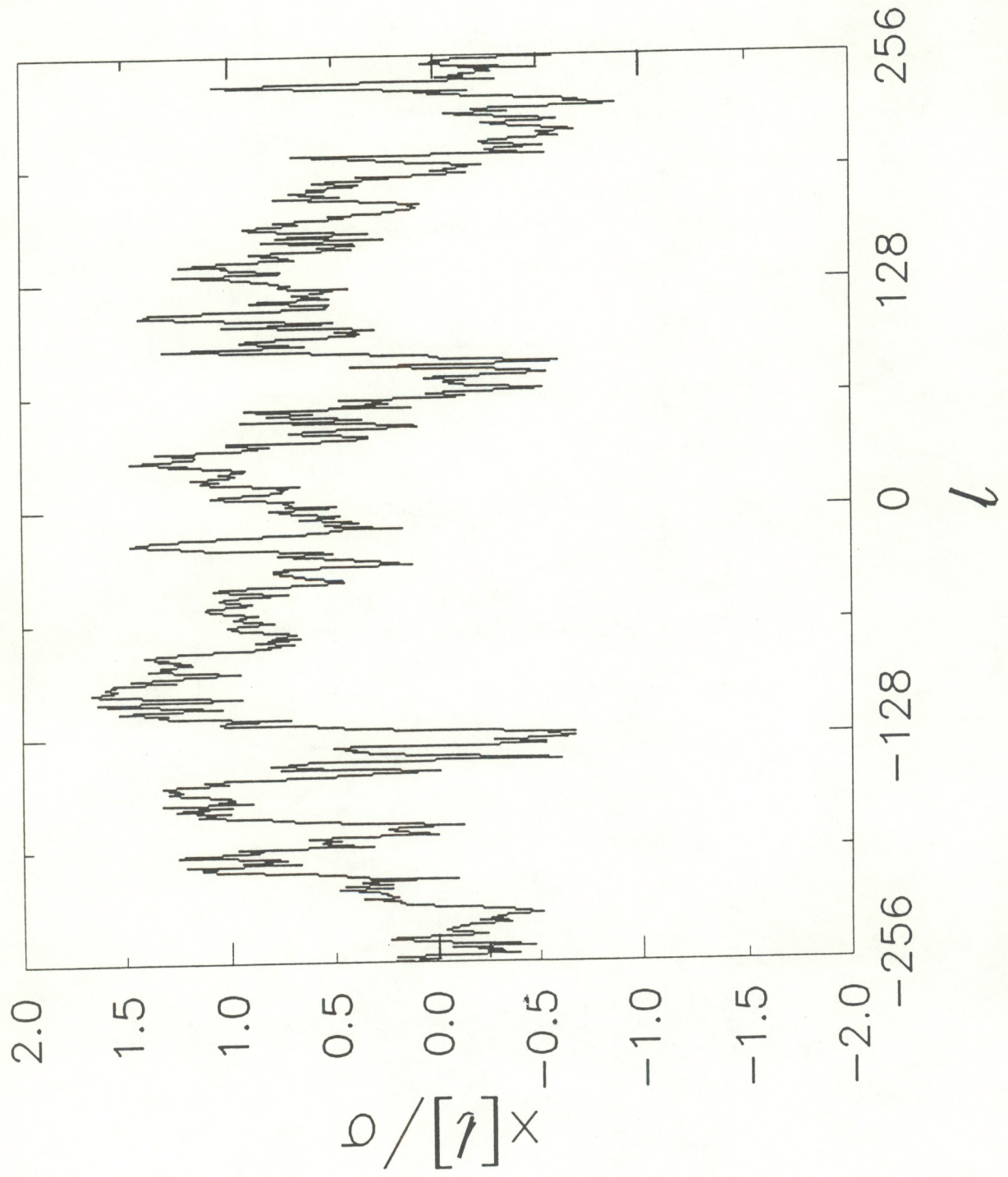

Fig. 7. A 512 point sample segment from the aircraft longitudinal air velocity data $x[\ell] = x(\ell\Delta t)$, normalized by the standard deviation σ of the entire 16,384 point series, as function of the dimensionless time $\ell = t/\Delta t$ of that particular sample.

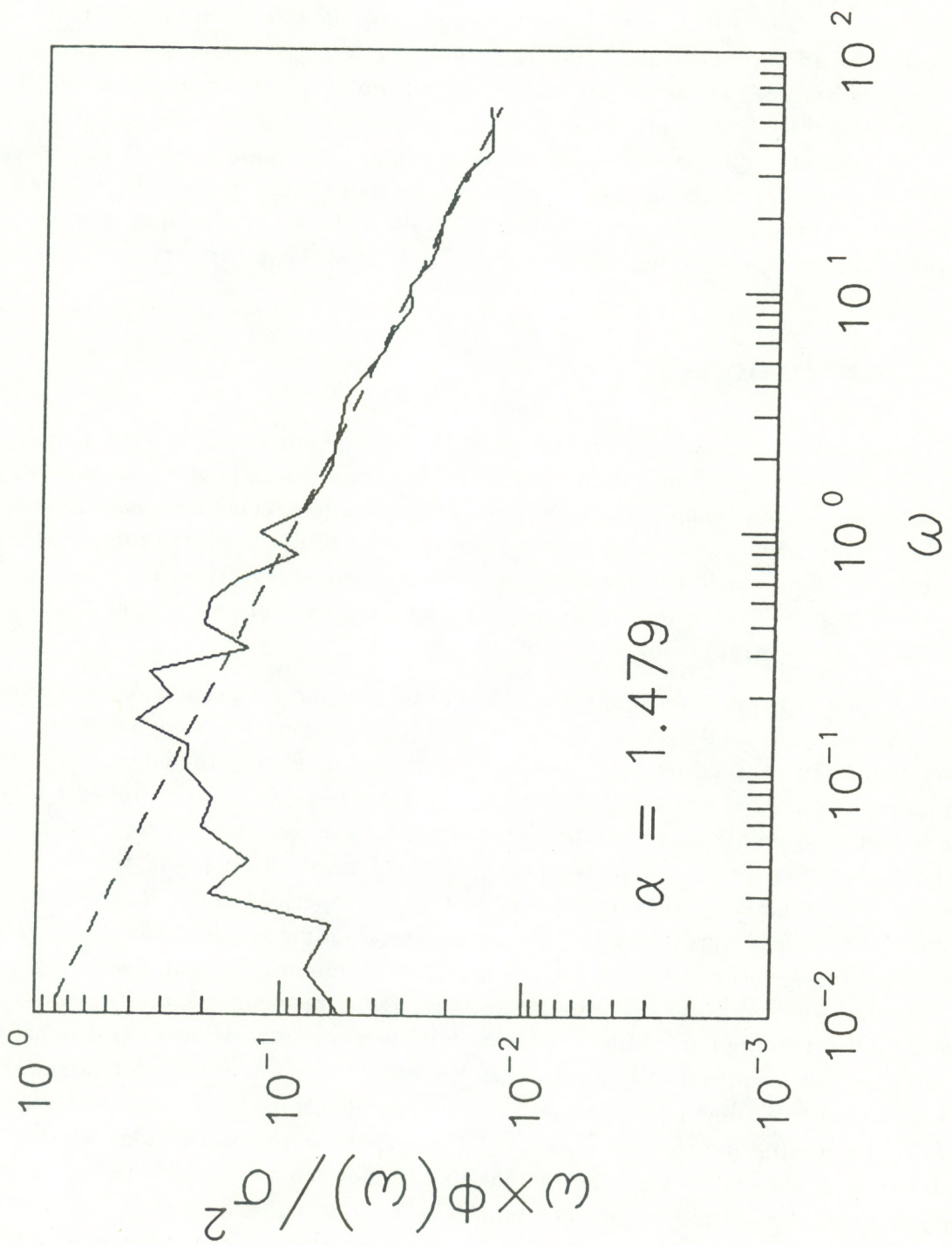

Fig. 8. Smoothed spectrum computed from four 16,384 point realizations of aircraft longitudinal air velocity data taken in the boundary layer. The dashed line is a log-log linear regression fit to the upper two frequency decades.

for the two windows were computed from the average spectra using the linear regression parameters (see Fig. 9). Note that the rectangular window is substantially below the theoretical line and the normalized Hanning window is slightly below the theoretical line in the range of harmonics from about 5 to 20. The ratio of the two pseudo-transfer functions (Fig. 10) is slightly below the theoretical line for harmonics greater than 2. It may be that the local slope of the actual spectrum of the data sample is slightly less than the regression fit in this frequency range or that there is some small effect because these time series do possess an integral scale. However, the final result is clear: the Hanning window produces a more accurate determination of the spectral power law than the rectangular window.

5 Conclusions

The characterization of geophysical variables by spectral analysis is an established practice. Typically we are looking for a significant scale (prominent peak in the spectrum) or a power law behavior in some frequency range that indicates a particular physical process. From a practical point of view, we must take a discrete series of data points (spatial or temporal) and process them to obtain an estimate of the intrinsic spectrum of the system. The way we preprocess the data before applying a Fourier analysis routine can greatly influence the fidelity of our spectral estimate.

In this paper we examined the specific issue of tapering the data series to improve estimates of a signal characterized by a variance spectrum with a power law behavior, $A|\omega|^{-\alpha}$. We first developed a general relationship, given by (16) and (17), between the intrinsic spectrum and the finite, discrete spectrum after tapering. These expressions were simplified by letting the number of data points go to infinity. This allowed us to deal with finite, continuous series without worrying about the well-understood problem of aliasing. We then examined the specific application of a rectangular window (i.e., no tapering) and a Hanning window to a signal characterized by a power law spectrum. The Hanning window was found to faithfully reproduce the spectrum, except for the first few harmonics, for α between -1 to 3. The rectangular window gives the proper spectrum for α between -1 and 1. For α between 1 and 2, the rectangular window substantially overestimates the spectral density at low harmonics, but asymptotically approaches the proper value as k becomes large. For $\alpha = 2$, the rectangular window overestimates the intrinsic spectrum by a constant factor of 2; for $\alpha > 2$, the results diverge as k increases. This effect for the rectangular window is easily understood if we realize that the rectangular window chops a segment out of the signal leaving sharp discontinuities at each end. The Fourier series of a step function (i.e., the discontinuity) yields a spectrum with a frequency to the -2 dependence, which becomes superimposed on the spectrum of the signal of interest, thus explaining the transition of behavior that occurs at α equal to 2.0. These results were verified for discrete analysis by processing synthetic data series of several different power laws and an actual atmospheric data series characterized by a spectrum with a high-frequency subrange with $\alpha \simeq 1.5$.

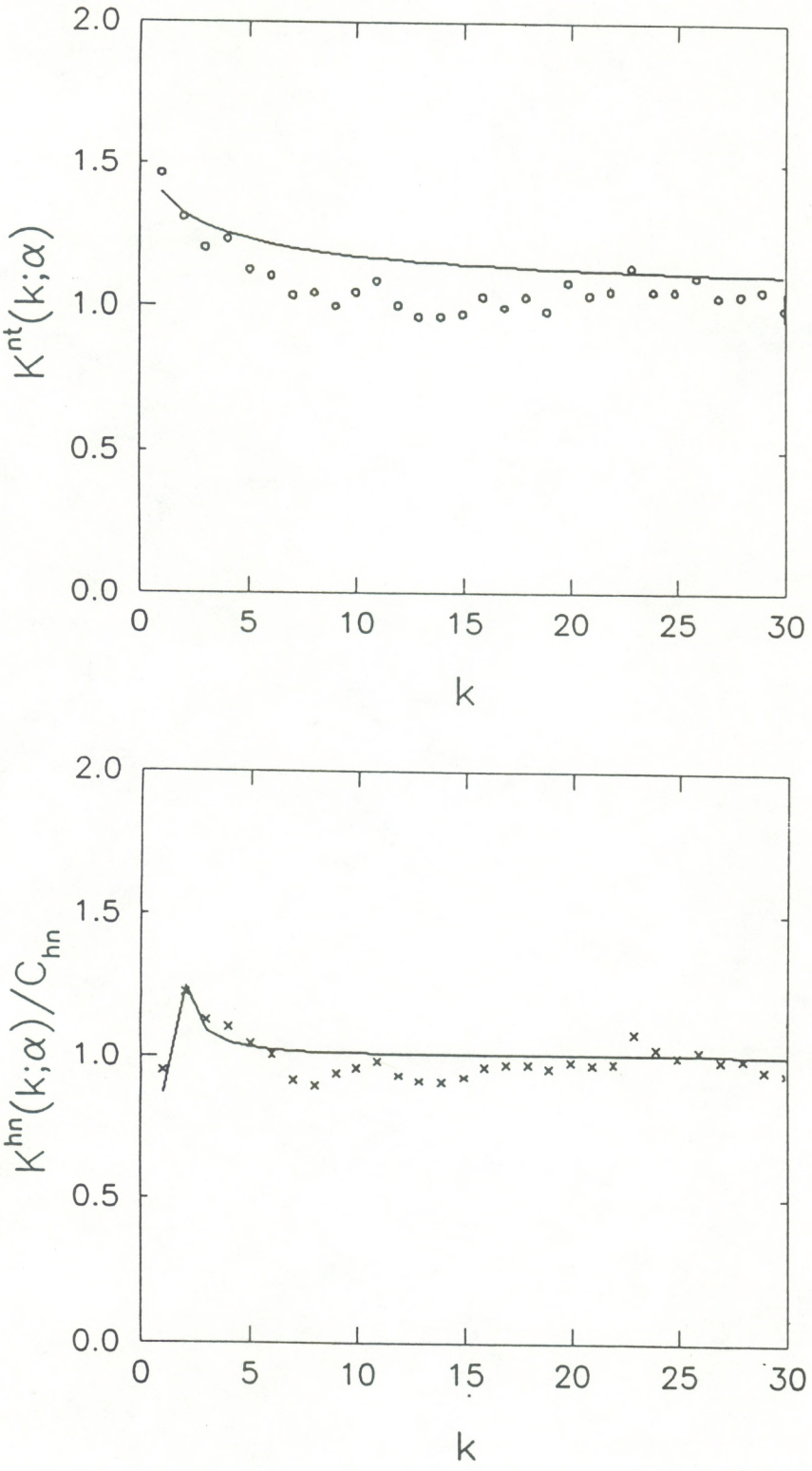

Fig. 9. Normalized pseudo-transfer functions versus harmonic index for the aircraft data: (a) rectangular window, (b) Hanning window. The solid line is the theoretical prediction.

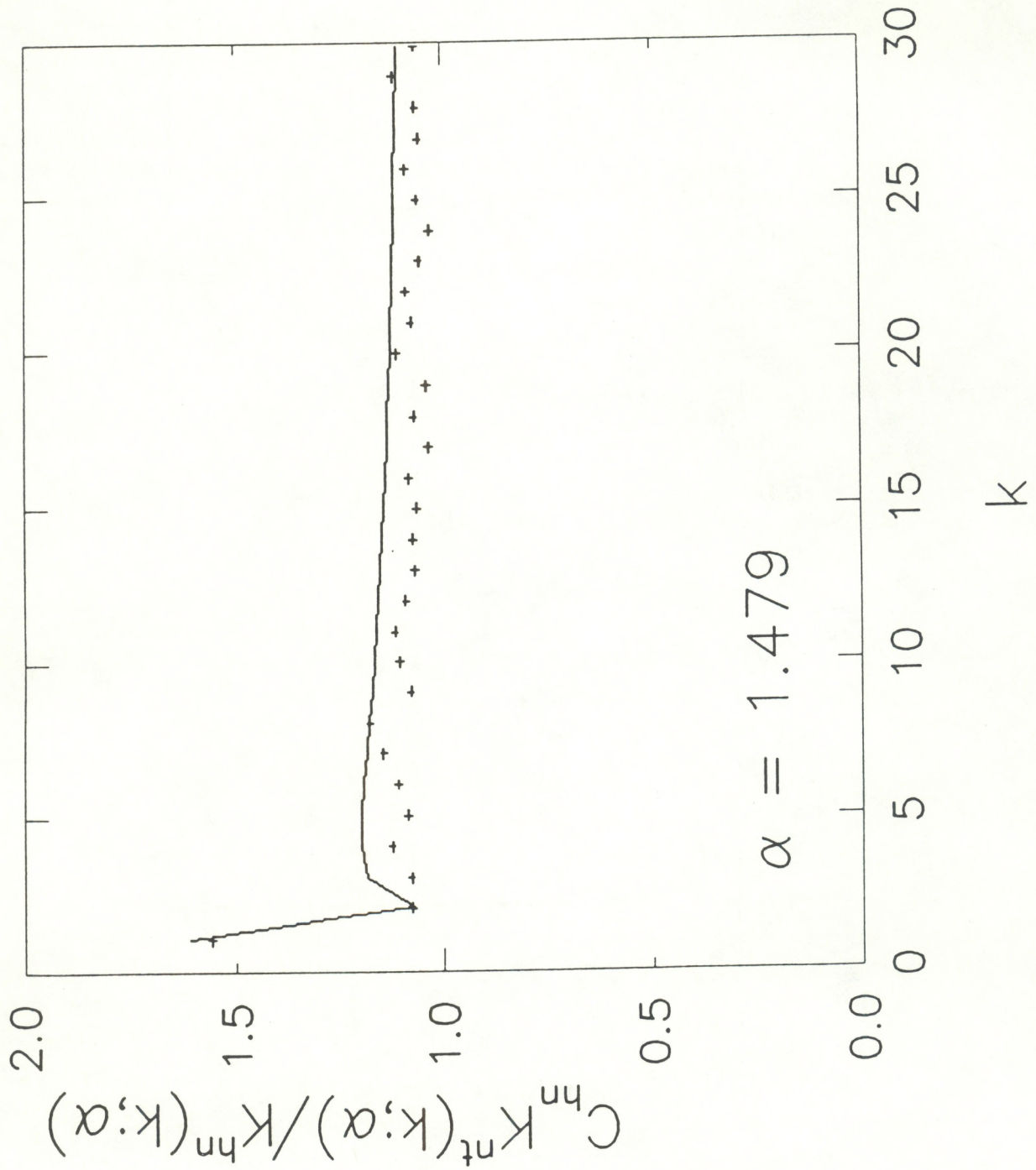

Fig. 10. Ratio of the rectangular to the normalized hanning pseudo-transfer functions versus harmonic for the aircraft data. The solid line is the theoretical prediction.

This study has also revealed a more subtle point regarding the proper normalization for the spectrum obtained with the tapering window. It is common practice to normalize the spectral density by the ratio of the variance of the time series computed before (rectangular window) and after application of a tapering window. This ensures that the tapered spectrum will sum to the same total variance as the untapered spectrum. This ratio is the quantity $Q(\alpha)$ discussed in section 3 [(68) and (69)]. However, we also showed in subsection 2.3 that dividing the tapered signal spectrum by the area (33) under the square of the window yields the correct estimate of the intrinsic spectral density. In the case of a power law spectrum, these two approaches are in agreement only for $\alpha < 1$. For $\alpha > 1$, normalization by the variance ratios results in erroneous spectral values and the error increases with increasing α (recall Fig. 3). This apparent paradox is resolved when we realize that the rectangular window does not produce the intrinsic variance of the signal [recall it produces the integral of the spectrum weighted by $1 - \mathrm{sinc}^2(\omega T/2)$]. In fact, it does not produce even a proper estimate of the variance of the signal in the frequency band of the analysis (i.e., between the fundamental and Nyquist frequencies) if $\alpha > 1$; a 100% error results for $\alpha = 2$. The tapered signal spectrum normalized by (33) does not produce the exact variance in the analysis band either, because of distortion of the first few harmonics, but the errors are much smaller than those with the rectangular window. Thus, we conclude that a spectrum computed with a tapering window should be normalized by the square of the window area and not by the ratio of the variances. The point about normalization of the spectrum by the square of the window area can be found in the literature on random signal analysis, but, considering its importance, it tends to be deeply buried. For example, in a 32-page paper on use of windows, Harris (1978) does not mention it. Priestly (1981) withholds this tidbit until page 559 and Bendat and Piersol (1971) mention it briefly on page 323 but erroneously state that we should normalize by the area of the window (rather than the area of the square of the window). Incidentally, many of these same textbooks recommend the 10% cosine tapering window, which Kaimal and Kristensen (1990) showed to be a poor choice.

Finally, we should mention that there are at least two alternatives to tapering the time series. As we discussed earlier, if an integral scale exists, a rectangular window can be used if the interval is increased until it is much larger than the integral scale. A second approach is to "prewhiten" the spectrum (Blackman and Tukey 1958). For example, the first derivative of the time series is equivalent to multiplying the variance spectrum by ω^2. Hence, a signal with $\alpha \simeq 5/3$ would be converted to a spectral density of $\alpha \simeq -1/3$. Then the use of a rectangular window would result in little error. However, both alternatives require some knowledge of the spectrum, whereas the tapering approach does not.

Acknowledgements. We acknowledge the support of the NCAR Research Aviation Facility in carrying out the Electra flight that was used for the example discussed here, and the assistance of John DeSanto in processing data from the flight. Also, we appreciate the useful comments by R.J. Lataitis.

REFERENCES

Anderson, R.V., 1977: Atmospheric electricity in the real world, *Electrical Processes in Atmospheres,* Steinkopf Verlag, 87-99.

Anderson, R.V., 1982: The dependence of space charge spectra on Aitken nucleus concentrations, *J. Geophys. Res.,* **87**, 1216-1218.

Bendat, J.S., and A.G. Piersol, 1971: *Random Data: Analysis and Measurement Methods,* Wiley-Interscience, 406 pp.

Blackman, R.B., and J.W. Tukey, 1958: *The Measurement of Power Spectra,* Dover Publications, 190 pp.

Charney, J.G., 1971: Geostrophic turbulence, *J. Atmos. Sci.,* **28**, 1087-1095.

Fairall, C.W., and S.E. Larsen, 1986: Inertial dissipation methods and turbulent fluxes at the air ocean interface, *Bound.-Layer Meteor.,* **34**, 287-301.

Fairall, C.W., J.B. Edson, S.E. Larsen, and P.G. Mestayer, 1990: Inertial-dissipation air-sea flux measurements: A prototype system using realtime spectral computations, *J. Atmos. Oceanic Technol.,* **7**, 425-453.

Hamming, R.W., 1977: *Digital Filters,* Prentice-Hall, 226 pp.

Harris, F.J., 1978: On the use of windows for harmonic analysis with the discrete Fourier transform, *Proc. of the IEEE,* **66**, 51-83.

Hasse, L, 1985: Comments on "A note on time averages in turbulence with reference to geophysical applications", *Tellus,* **37B**, 313-314.

Kaimal, J.C., 1978: Horizontal velocity spectra in an unstable surface layer, *J. Atmos. Sci.,* **35**, 18-24.

Kaimal, J.C., and J.E. Gaynor, 1983: The Boulder Atmospheric Observatory, *J.Clim. Appl. Meteor.,* **22**, 863-880.

Kaimal, J.C., S.F. Clifford, and R.J. Lataitis, 1989: Effect of finite sampling on atmospheric spectra, *Bound.-Layer Meteor.,* **47**, 337-347.

Kaimal, J.C., and L. Kristensen, 1990: Finite sampling, windowing, and the estimation of dissipation rates, *Proc. 9th Symposium on Turbulence and Diffusion,* Roskilde, Denmark, April 30 – May 3, Amer. Meteor. Soc., Boston, MA, 25-28.

Kraichnan, R.H., 1967: Inertial ranges in two-dimensional turbulence, *Phys. Fluids,* **10**, 1417-1423.

Kristensen, L., D.H. Lenschow, P. Kirkegaard, and M Courtney, 1989: The spectral velocity tensor for homogeneous boundary layer turbulence, *Bound.-Layer Meteor.,* **47**, 149-193.

Kristensen, L., and P. Kirkegaard, 1989: Comments on "Effects of finite sampling on atmospheric spectra", *Bound.-Layer Meteor.,* **48**, 205-210.

Lenschow, D. H., 1986: Aircraft measurements in the boundary layer, *Probing the Atmospheric Boundary Layer*, American Meteorological Society, Boston, MA, 39-55.

Lumley, J.L., and H.A. Panofsky, 1964: *Atmospheric Turbulence*, Interscience Monographs and Texts in Physics and Astronomy, John Wiley & Sons, 239 pp.

Panofsky, H.A., and J.A. Dutton, 1984: *Atmospheric Turbulence,* John Wiley & Sons, 397 pp.

Pasquill, F., and F.B. Smith, 1983: *Atmospheric Diffusion,* 3rd Edition, Ellis Horwood Ltd., 437 pp.

Priestly, M.B, 1981: *Spectral Analysis and Time Series,* Academic Press, 877 pp.

Sidi, C., J. Lefrere, F. Dalaudier, and J. Barat, 1988: An improved atmospheric buoyancy wave model, *J. Geophys. Res.,* **93**, 774-790.

Tennekes, H., and J.L. Lumley, 1972: *A First Course in Turbulence,* MIT Press, 300 pp.

A The integral $T(\alpha; m.n)$

We discuss the computation of the following integral, introduced in the main text:

$$T(\alpha;m,n) = \pi^{\alpha-1}\int_0^\infty u^{-\alpha}\{\mathrm{sinc}(u+m\pi)\mathrm{sinc}(u+n\pi) + \mathrm{sinc}(u-m\pi)\mathrm{sinc}(u-n\pi)\}\,du, \tag{A1}$$

where we allow m and n to assume any integral values (positive, negative, or zero), and where α is a real parameter. The convergence range for α depends on m and n in the following way:

$$m \neq 0 \quad \vee \quad n \neq 0: \qquad \alpha \in (-1,3) \tag{A2}$$

$$m = 0 \quad \wedge \quad n = 0: \qquad \alpha \in (-1,1) \tag{A3}$$

We will show that $T(\alpha;m,n)$ can be expressed in terms of the functions

$$s(x,\alpha) = \int_0^x t^{\alpha-1}\sin t\,dt \tag{A4}$$

and

$$c(x,\alpha) = \int_0^x t^{\alpha-1}\cos t\,dt, \tag{A5}$$

which may be regarded as generalizations of the well-known sine and cosine integral functions

$$\mathrm{Si}(x) = \int_0^x \frac{\sin t}{t}dt \tag{A6}$$

and

$$\mathrm{Ci}(x) = -\int_x^\infty \frac{\cos t}{t}dt. \tag{A7}$$

The analysis splits into two parts, one for $m \neq n$, and one for $m = n$.

Main case I: $m \neq n$
Using the decomposition

$$\mathrm{sinc}(u+m\pi)\mathrm{sinc}(u+n\pi)+\mathrm{sinc}(u-m\pi)\mathrm{sinc}(u-n\pi)=$$

$$\frac{(-1)^{m+n}}{(n-m)\pi}\left(\frac{1}{u+m\pi}-\frac{1}{u-m\pi}-\frac{1}{u+n\pi}+\frac{1}{u-n\pi}\right)\sin^2 u \tag{A8}$$

we get

$$T(\alpha;m,n)=\pi^{\alpha-2}\frac{(-1)^{m+n}}{n-m}\{J(m,\alpha)-J(-m,\alpha)-J(n,\alpha)+J(-n,\alpha)\}, \tag{A9}$$

where we have introduced the fundamental integral

$$J(m,\alpha)=\int_0^\infty \frac{\sin^2 u}{u+m\pi}u^{-\alpha}\,du. \tag{A10}$$

Because any terms with $m=0$ or $n=0$ cancel in (A9), we need consider only $m\neq 0$; let us first assume $m>0$. The basic idea is to replace the discrete function $J(m,\alpha)$ by a function of a continuous variable x. We define

$$h(x,\alpha)=\int_0^\infty \frac{\sin^2(x\{1+t\})}{1+t}t^{-\alpha}\,dt, \tag{A11}$$

such that we have

$$x^{-\alpha}h(x,\alpha)=J(m,\alpha) \tag{A12}$$

on making the identification

$$x=m\pi. \tag{A13}$$

By differentiation of (A6), we get

$$\frac{\partial}{\partial x}h(x,\alpha)=\int_0^\infty\{\sin(2x)\cos(2xt)+\cos(2x)\sin(2xt)\}t^{-\alpha}\,dt, \tag{A14}$$

which reduces to

$$\frac{\partial}{\partial x}h(x,\alpha)=2^{\alpha-1}\Gamma(1-\alpha)x^{\alpha-1}\{\sin(\pi\alpha/2)\sin(2x)+\cos(\pi\alpha/2)\cos(2x)\}. \tag{A15}$$

The right-hand side can be integrated in terms of the functions (A4) and (A5):

$$h(x,\alpha) = \frac{1}{2}\Gamma(1-\alpha)\{\sin(\pi\alpha/2)s(2x,\alpha) + \cos(\pi\alpha/2)c(2x,\alpha)\}. \tag{A16}$$

The case $m < 0$ is treated in an analogous fashion, and the two cases are united in the following expression valid for all $m \neq 0$:

$$\begin{aligned} J(m,\alpha) &= \frac{1}{2}\Gamma(1-\alpha)(|m|\pi)^{-\alpha}\{\mathrm{sgn}(m)\sin(\pi\alpha/2)s(2|m|\pi,\alpha) \\ &\qquad + \cos(\pi\alpha/2)c(2|m|\pi,\alpha)\}, \end{aligned} \tag{A17}$$

where $\mathrm{sgn}(m) = 1$ for $m > 0$ and $\mathrm{sgn}(m) = -1$ for $m < 0$. When we insert (A17) in (A9) and apply the reflection rule

$$\Gamma(1-\alpha)\Gamma(\alpha) = \frac{\pi}{\sin(\pi\alpha)}, \tag{A18}$$

we achieve the result

$$\begin{aligned} T(\alpha;m,n) &= \frac{(-1)^{m+n}}{n-m}\frac{1}{2\pi\Gamma(\alpha)\cos(\pi\alpha/2)} \\ &\qquad \times \{\mathrm{sgn}(m)|m|^{-\alpha}s(2|m|\pi,\alpha) - \mathrm{sgn}(n)|n|^{-\alpha}s(2|n|\pi,\alpha)\}. \end{aligned} \tag{A19}$$

If either m or n is 0, then the corresponding term in the braces of (A19) should be interpreted as zero. Inside the α-convergence interval $(-1,3)$ are three integral values of α, namely, $\alpha =$ 0, 1, and 2. Without difficulty we find

$$T(0;m,n) = 0 \tag{A20}$$

and

$$T(2;m,n) = \frac{(-1)^{m+n}}{mn}. \tag{A21}$$

The case of $\alpha = 1$ is more difficult. Here (A19) fails to give the answer directly, but it can be used in a limit analysis that leads to

$$T(1;m,n) = \frac{(-1)^{m+n}}{(n-m)\pi^2}\{\varphi(m) - \varphi(n)\}, \tag{A22}$$

where

$$\varphi(m) = \begin{cases} 0 & m = 0 \\ \{\gamma + \ln(2|m|\pi) - \mathrm{Ci}(2|m|\pi)\}/m & m \neq 0, \end{cases} \tag{A23}$$

γ being Euler's constant.

Main case II: $m = n$
When $m = 0$ we find

$$T(\alpha;0,0) = \frac{(2\pi)^\alpha}{\cos(\pi\alpha/2)\Gamma(2+\alpha)}, \tag{A24}$$

holding for $\alpha \in (-1,1)$, cf. (A3). Next suppose $m > 0$. We introduce the continuous function

$$k(x,\alpha) = \int_0^\infty \left\{ \frac{\sin^2(x\{1-t\})}{(1-t)^2} + \frac{\sin^2(x\{1+t\})}{(1+t)^2} \right\} t^{-\alpha}\, dt, \tag{A25}$$

where now

$$\pi^{\alpha-1}x^{-\alpha-1}k(x,\alpha) = T(\alpha;m,m), \tag{A26}$$

but still with the connection of x and m given in (A13). Differentiation of (A25) twice leads to

$$\frac{\partial^2}{\partial x^2}k(x,\alpha) = 2\int_0^\infty \{\cos(2x\{1-t\}) + \cos(2x\{1+t\})\}t^{-\alpha}\, dt, \tag{A27}$$

which reduces to

$$\frac{\partial^2}{\partial x^2}k(x,\alpha) = 2^{\alpha+1}\Gamma(1-\alpha)\sin(\pi\alpha/2)x^{\alpha-1}\cos(2x). \tag{A28}$$

As a first integral we obtain

$$\frac{\partial}{\partial x}k(x,\alpha) = 2\Gamma(1-\alpha)\sin(\pi\alpha/2)c(2x,\alpha); \tag{A29}$$

integration once more, with application of the formula

$$\int_0^x c(t,\alpha)\, dt = xc(x,\alpha) + \alpha s(x,\alpha) - x^\alpha \sin x, \tag{A30}$$

yields

$$k(x,\alpha) = \Gamma(1-\alpha)\sin(\pi\alpha/2)\{2xc(2x,\alpha) + \alpha s(2x,\alpha) - (2x)^\alpha \sin(2x)\}. \tag{A31}$$

By combining (A31), (A26), (A13), and (A18), we conclude

$$T(\alpha;m,m)=\frac{|m|^{-\alpha}}{\cos(\pi\alpha/2)\Gamma(\alpha)}\left\{c(2|m|\pi,\alpha)+\frac{\alpha}{2\pi|m|}s(2|m|\pi,\alpha)\right\}. \tag{A32}$$

With the formula written in this form, we also cover the case $m<0$ because $T(\alpha;-m,-m)=T(\alpha;m,m)$. Again we want to discuss the integral values of α separately. The cases $\alpha=0$ and $\alpha=2$ are easy, and we get

$$T(0;m,m)=1 \tag{A33}$$

and

$$T(2;m,m)=\frac{2}{m^2}. \tag{A34}$$

A little more analysis is needed for $\alpha=1$:

$$T(1;m,m)=\frac{1}{(m\pi)^2}\{2|m|\pi\,\mathrm{Si}(2|m|\pi)+\gamma+\ln(2|m|\pi)-\mathrm{Ci}(2|m|\pi)\}. \tag{A35}$$

We have reduced the computation of $T(\alpha;m,n)$ to evaluation of the generalized sine and cosine integral functions s and c defined by (A4) and (A5). Numerical computations of $s(x,\alpha)$ and $c(x,\alpha)$ are for small x carried out by the Taylor series for these functions, whereas for large x we use the asymptotic expansions, which for $x=2m\pi$ reduce to

$$\begin{aligned} s(2m\pi,\alpha) &\sim \sin(\pi\alpha/2)\Gamma(\alpha) \\ &\quad -(2m\pi)^{\alpha-1}\sum_{m=0}^{\infty}(-1)^m\frac{(\alpha-1)(\alpha-2)\ldots(\alpha-2m)}{(2m\pi)^{2m}} \end{aligned} \tag{A36}$$

and

$$\begin{aligned} c(2m\pi,\alpha) &\sim \cos(\pi\alpha/2)\Gamma(\alpha) \\ &\quad +(2m\pi)^{\alpha-1}\sum_{m=0}^{\infty}(-1)^m\frac{(\alpha-1)(\alpha-2)\ldots(\alpha-2m-1)}{(2m\pi)^{2m+1}}. \end{aligned} \tag{A37}$$

Notice that the integral defining $c(x,\alpha)$ in (A5) converges only for $\alpha>0$, but as (A2) - (A3) show, negative values of α should be admitted. This is no serious problem, because both functions $s(x,\alpha)$ and $c(x,\alpha)$, qua their relationship with the incomplete gamma function, can be continued analytically to negative α-values in a way that preserves the validity of our numerical algorithms. Similarly, though the intermediate integrals (A12) and (A25) converge only for $\alpha\in(0,1)$, our final results can be used for any α in the convergence range of the original integral (A1). Again, this is so because of the analytical continuation.

Asymptotic expressions

The two pseudo-transfer functions $K^{\mathrm{nt}}(k;\alpha)$ and $K^{\mathrm{hn}}(k;\alpha)$ are expressible in terms of the T function, as equations (60) and (63) show. To find asymptotic forms of these transfer functions when k is large, we use the asymptotic expansions of the constituent functions $s(2m\pi,\alpha)$ and $c(2m\pi,\alpha)$ given in (A36) and (A37), retaining only the leading terms with $m = 0$. To cover the case $\alpha = 1$ we also need the expansion

$$\mathrm{Ci}(2m\pi) \sim \sum_{m=0}^{\infty} (-1)^{m+1} \frac{(2m+1)!}{(2m\pi)^{2m+2}} \quad . \tag{A38}$$

Proceeding in this way, a straightforward calculation gives the asymptotic form (62) of $K^{\mathrm{nt}}(k;\alpha)$, from which (61) follows. The Hanning case $K^{\mathrm{hn}}(k;\alpha)$ is more cumbersome; we let the computer-algebra program REDUCE do the arithmetic. In the intermediate computations we used the truncated binomial series

$$\left(1+\frac{1}{k}\right)^{\alpha} \approx \sum_{r=0}^{m} \binom{r}{\alpha} \left(\frac{1}{k}\right)^{r}, \tag{A39}$$

with $m = 2$. The final asymptotic result turned out to be (64), and numerical experiments show that even for moderate values of k this formula is a very accurate approximation to (63).

*U.S. GOVERNMENT PRINTING OFFICE: 1992-673-025/69024